LIFE17 ENV/FR/000398 LIFE ADSORB project is supported by the European Union LIFE program
Le projet LIFE17 ENV/FR/000398 LIFE ADSORB bénéficie du soutien financier du programme LIFE de l'Union européenne

LIFE ADSORB

LIFE17 ENV/FR/000398

Deliverable B.2.1 : Report describing the modelling platform set up and the results of model calibration/validation

Reporting date

V1	June 2025
V2	January 2026

Table des matières

Abstract

This deliverable presents the modelling work carried out within the LIFE ADSORB project to simulate and analyze the hydraulic behavior and micropollutant transport in two treatment wetlands designed for stormwater management. The main objective was to develop a robust numerical model capable of representing the complexity of water flow and contaminant dynamics under varying weather and operational conditions.

The modelling platform was built using COMSOL Multiphysics, enhanced by custom MATLAB scripts to address specific features such as surface water flow and underdrain hydraulics. The two filters studied differ in their filtering media: Filter 1 is composed solely of sand, while Filter 2 incorporates a reactive layer (Rainclean®) between layers of sand, designed to enhance micropollutant adsorption.

To calibrate and validate the model, tracer tests were conducted in real field conditions under both dry and rainy weather operation modes. These experiments revealed significant heterogeneity in flow patterns, including preferential paths and stagnant zones, particularly in the absence of a well-distributed inlet or sufficient drainage network.

Simulation results demonstrated that micropollutants are better retained in Filter 2 due to the presence of Rainclean®, but also revealed a risk of desorption when the system receives cleaner water during dry periods. Alternating simulations of dry and wet weather confirmed a cyclic adsorption/desorption pattern, with implications for the long-term efficiency of the filters.

The study highlights the importance of a uniform inflow distribution and well-dimensioned drainage to optimize the use of the filter surface and reduce dead zones. Recommendations include avoiding abrupt changes in inflow pollutant concentrations and improving design features to sustain micropollutant retention performance over time.

The numerical model can be downloaded from the project website (https://life-adsorb.eu/), under the section. livrables/livrables B2/Développement et calage du modèle.

1 A review of the aims delineated in the proposal

In the context of the ADSORB project, the primary objective of mechanistic modeling is to enhance comprehension of the mechanisms that occur within the filters, striving for a representation that closely mirrors reality. The identification of the parameters impacting the flow, transport, and fate of micropollutants will be possible. A comparison of the results obtained from the mechanistic model with those obtained from ORAGE will allow for an evaluation of the extent to which simplified models such as ORAGE can be used to predict the functioning of the filters. It is anticipated that the implementation of a model will facilitate the adjustment of filter operation, thereby attaining optimal performance. Subsequently, the following will be possible: (i) prediction of the filters' fate at a time range that exceeds the project, taking into account the system's aging, and (ii) simulation of the filter's functioning when confronted with alternative scenarios (e.g., modification of rain event characteristics, different filter surfaces, outflow rate, and layer thicknesses).

2 Questions for research and selection of the numerical model

The numerical model under development aims to tackle two essential questions: (a) does the design ensure sufficient functionality and optimal use of the reactive material's volume? and (b) is there a potential for desorption when the inlet concentration changes or when the reactive material reaches saturation?

(a) From the onset of the project, concerns have arisen about the treatment wetland's design. The positioning of the feeding point at one end of the filter has come under scrutiny, as it may not ensure optimal distribution, particularly during dry spells. In addition, upon commencing the modeling work and reviewing the treatment wetland's design details, it was discovered that the unique configuration of the underdrains (see Figure 1) could lead to preferential flows through the porous media.

Figure 1. The merging of the two upstream underdrains into a singular section of the same size prompts inquiry regarding how this distinctive setup affects flow distribution throughout the underdrains.

(b) The use of adsorbent materials often brings up concerns about the risk of desorption (Toro-Vélez *et al.*, 2016, Qi *et al.*, 2018, Li *et al.*, 2020), particularly when the adsorption capacity is full, and the adsorbed pollutants have an extended half-life. The risk is further elevated when the inlet concentration varies, a condition probable in the studied system due to alternating dry and rainy periods (Zhu *et al.*, 2021, 2022).

To address these inquiries, a model is required that offers spatially distributed assessments of water pressure, velocity, and pollutant concentrations. Consequently, conceptual models (such as reservoir models) are unsuitable. Moreover, the absence of sufficient data precludes the use of machine learning techniques. Consequently, numerical modeling focused on discrete methods for solving partial differential equations, including finite elements and finite volumes, was selected.

Table 1. Open-source and commercial numerical models for porous media flow and transport simulation

Name	Method	License	Capabilities
HYDRUS (PC Progress)	Finite elements	Commercial	Simulates flow, heat, and solute transport in variably saturated porous media.
FEFLOW (DHI)	Finite elements	Commercial	Models groundwater flow, contaminant transport, and heat transport in saturated and unsaturated porous media.
COMSOL Multiphysics	Finite elements	Commercial	Simulates flow and transport in porous media, including Darcy, Brinkman, and multiphase flow
ANSYS Fluent	Finite volumes	Commercial	Models flow and transport in porous media, with options for multiphase and reactive transport
OpenFoam	Finite volumes	Open-Source	Includes both built-in and community-developed solvers (like RichardsFoam) for simulating variably saturated flow in porous media.

Table 1 offers a selective compilation of key commercial and open-source software tools designed for simulating flow and transport in porous media using discrete numerical methods. Our decision to utilize COMSOL Multiphysics is based on the following: (i) successful development of treatment wetland models has already been achieved with it (Rajabzadeh *et al.*, 2015, Samso *et al.*, 2015, 2016) and (ii) it can be integrated with MATLAB to leverage specific functions that replicate the behavior of distinct elements, such as surface or underdrain flows.

2.1 Domain geometry simplification

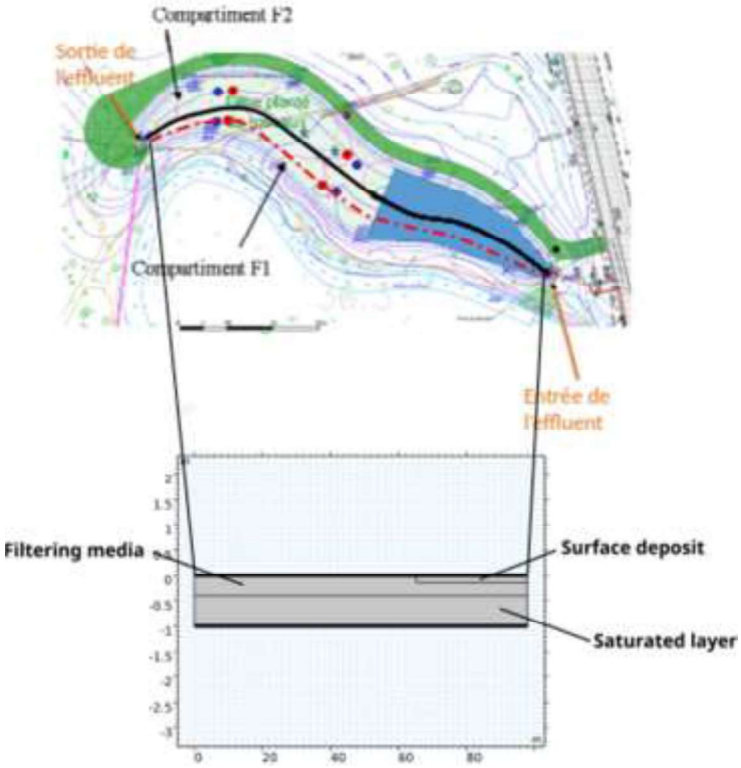

Figure 2. Domain geometry simplification. The upper diagram shows a plan view of the filters from above. Due to the symmetry along each filter's centerline (indicated by a red dotted line for filter 1), we deduce a representative 2D cross-section, which is shown in the lower portion of the figure.

In this section, the focus is given on describing the geometrical assumption we made in order to reduce computation costs. A more detailed description of the studied site is given in Appendixe: Bugeaud treatment wetlands.

To decrease computational costs, an initial step involves simplifying the geometry by taking into account present symmetries. We presume that each filter exhibits symmetry along its longitudinal centerline, resulting in a simplified two-dimensional geometry (see Figure 2).

The longitudinal cross-section obtained (length of 98 m and a height of 1 m) has been constructed using the graphical user interface of COMSOL Multiphysics and is divided into three distinct layers, described as follows from top to bottom (see Figure 2):

- Surface Deposit: For scenarios reflecting the system's current state, its size has been assessed through local observation and measurement (deliverable task C1). It is estimated to cover one-third of the filter's length with a 15 cm thickness.
- Filtering Media (or Reactive Layer): Only sand is used for filter 1, while Rainclean® (20 cm) between two layers of sand (10 cm) are employed for filter 2. This layer is 40 cm thick.
- Drainage Layer: Situated just above the underdrain, this layer is made of fine and coarser gravel, extending vertically for 60 centimeters, representing the transition (10 cm) and drainage layers of the filters (50 cm).

Notwithstanding the simple geometry, meshing proved to be a major challenge, especially for filter 2, due to the thin layers of material compared to the length of the system. Furthermore, the presence of sharp pressure gradients near the inlet necessitated careful consideration, and the mesh was refined in the inlet vicinity to ensure accuracy and model stability. The resulting mesh comprises 34,830 meshes, with an average quality of 0.85[1].

2.2 Operation of the filters

The filters are fed in an alternating manner. The alternance occurring on a monthly basis. The system has been configured to operate in three distinct modes, each tailored to specific volumes of water present within the pumping station. These modes are designated as follows: "dry weather", "rain weather", and "storm events". In instances wherein the storage capacity of the pumping station exceeds 3,500 m^3, the overflow of stormwater to the Seine River is initiated.

2.2.1 Dry weather operation

In this operation mode, the filter currently in use is fed at a rate of six times per day by a batch with a volume of 120 m^3. The duration of each batch is 59 minutes, and the flow rate is 33.6 L/s. Consequently, the daily hydraulic load is 720 m^3/d.

2.2.2 Rain weather operation

The filter is fed in two steps during the "rain weather" mode. Firstly, the filter in operation is fed at a flow rate of 70 L/s up to a level known as ‘high ponding’ level (0.97 and 1.06 m from the bottom of filters 1 and 2, respectively). Once this level is reached, the feed is stopped until the water level in the filter reaches a so-called ‘low ponding’ level (0.93 and 0.97 m from the bottom of filters 1 and 2, respectively). Once this level is reached, the filter is fed again to maintain the water level, at a flow rate of 40.1 L/s, up to the ‘high ponding’ level. Here again, the feed is stopped until the water level in the filter reaches the ‘low ponding’ level. The alternation between ‘high ponding’ level and ‘low ponding’ level continues until the ‘rain weather’ operating mode is deactivated (when the level in the pumping station returns to the ‘pump stop level’ (0 m^3) or the ‘storm event’ level (1000 m^3) is exceeded).

2.2.3 Storm event operation

The ‘storm event’ operating mode occurs when the volume in the pumping station exceeds 1000 m^3. The two filters are fed simultaneously in parallel, with a flow rate of 100 L/s on the priority filter, then 70 L/s once the ‘high ponding’ level has been reached, and a flow rate of 35 L/s or 70 L/s (depending on the availabililowty of pumps and the water level in this filter) on the secondary filter. The water exits through the calibrated orifice of each filter. The ‘storm event’ operating mode is stopped when the level in the pumping station returns to the ‘pump stop level’ (0 m^3).

The operating phases of the ‘storm event’ mode are similar to those of the ‘rain weather’ mode for the two filters fed in parallel.

2.3 Modification of the numerical model

In order to address the unique characteristics of the system and to respond to the inquiries detailed in the section "Questions for research and selection of the numerical model," the abilities

[1] In COMSOL Multiphysics, the mesh quality is a metric ranging from 0 to 1, representing the equiangular skew, that is, the deformation relative to a hypothetical perfect equilateral triangle. The closer the value approaches 1, the more closely it aligns with an equilateral triangle.

of the numerical model, derived from the subsurface flow module in COMSOL Multiphysics, have been enhanced using custom MATLAB scripts.

2.3.1 The underdrain model

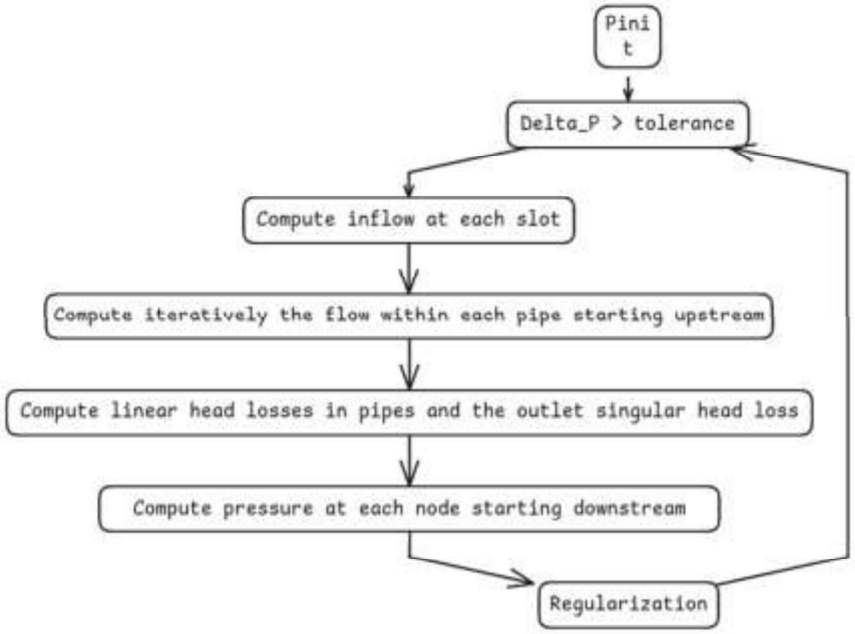

Figure 3. Analog model flow chart

To determine whether the size of the underdrain influences how flow is distributed within the filtering media, we initially chose to construct an analog model of the drain and monitor the flow distribution along the drain slots, assuming an ideally uniform distribution of water across the surface of the filter. Figure 3 shows the different calculation steps of the analog model. Since flow and pressure are interdependent, a loop is implemented. First, the pressure in the underdrain for all slots is set to a constant value. Then the algorithm calculates the inflow through each slot from upstream to downstream of the underdrain network. These values are used to calculate the flow along the entire underdrain to the outlet. Knowing the flow rate, the linear head losses between the slots are then estimated. Finally, the pressure values are updated based on the linear head losses starting downstream. The loop continues until the differences between the slot level pressures obtained in the previous iteration and those obtained in the current iteration are less than a given threshold (tolerance). A regularization term is introduced to limit deviation from the previous iteration and ensure that the model converge.

Using this analog model we demonstrated that the flow rate through the slots significantly varies along the underdrain depending on the saturation level of the filter (see Figure 4). It results in the formation of preferential paths near the outlet of the filter.

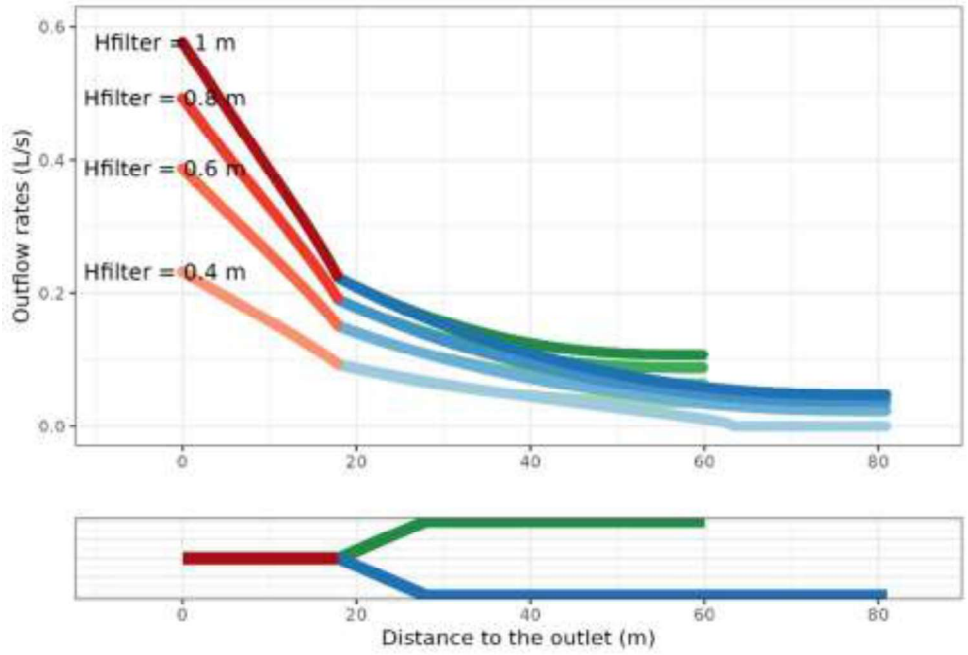

Figure 4. Distribution of simulated flow rates across each slot of the underdrain network as a function of its distance to the underdrain network outlet for different water heights in filter 1 (rugosity k = 1.5.10^{-6} m).

The findings of this section have been published in a scholarly journal article: Morvannou *et al.* (2023).

As a result, it was decided that the developed analog model need to be coupled with the porous media model to achieve a realistic representation of the flow in the filters.

2.3.2 The surface flow model

The integration of surface and subsurface flow remains a persistent obstacle in the field of hydrological sciences, leading to the development of numerous methodologies to address it (Meles *et al.*, 2024, Bittelli *et al.*, 2015, Weill *et al.*, 2009). The primary obstacles involve mass-balance concerns and numerical instabilities linked to this integration. Nonetheless, the majority of commercial software lacks this capability, and COMSOL is also part of this trend.

To address this problem, we implemented a one-dimensional finite difference model in MATLAB to solve the Manning-Stricker equations. The system of partial differential equations to be solved comprises:

$$\begin{cases} \frac{\partial h_s}{\partial t} + \frac{\partial h_s U_s}{\partial x} = q_s \\ U_s = -\frac{{h_s}^{2/3}}{n}\sqrt{\frac{\partial h_s}{\partial x}} \end{cases}$$

Equation 1

Where h_s is the water depth [L], U_s is the depth-averaged velocity [L.T^{-1}], q_s is the source/sink term [L.T^{-1}] and n is the coefficient of Manning-Stricker. A numerical solver employing an explicit finite difference approach has been developed in MATLAB.

2.3.3 Coupling in COMSOL Multiphysics

The integration of COMSOL Multiphysics and MATLAB-embedded numerical models has been facilitated by the MATLAB LiveLink toolbox. Throughout this integration process, we encountered

a few challenges: (i) utilizing uniform time steps across all three models is not feasible, (ii) memory writing operations need to be minimized to prevent a rise in computation time, and (iii) calls to MATLAB functions must also be restricted to avoid increased computation time.

2.4 The hydraulic model

The hydraulic model chosen to describe the flows in the layers described above is the Richards model, taking into account the Van Genuchten and Mualem equations (van Genuchten, 1980).

In order to obtain a set of hydraulic parameters that best reproduce the hydraulic behaviour of the filter containing only sand (filter 1), a parametric analysis was carried out on the parameter that takes into account the surface roughness (parameter n of the Manning-Strikler equation) as well as on the hydraulic parameters of the deposit and sand layers (Ks deposit, Ks sand, θs deposit, α deposit, α sand). An initial estimate of the hydraulic conductivities at saturation (Ks) were carried out in the laboratory with 6 samples taken (100 cm^3 cylinders) from the filter containing Rainclean® (filter 2) at rest in 2022, one year after the filters were commissioned (Table 2).

Table 2. Hydraulic conductivity values at saturation measured in the laboratory for various materials taken from the filter containing Rainclean®.

Location	Upstream piezometer 1			Middle piezometer		Downstream piezometer
Media	Deposit	Sand under deposit	Rainclean®	Sand with 1 cm of deposit	Rainclean®	Sand
K_s at 21°C (m/s)	$2.55.10^{-4}$	$7.90.10^{-4}$	$1.73.10^{-3}$	$1.03.10^{-3}$	$2.04.10^{-3}$	$2.50.10^{-3}$

In addition, to determine the saturation water content of the materials, solid density and porosity measurements were carried out by pycnometry on samples of virgin materials (sand and Rainclean®). The sand had a solid density ρ = 2.61 g/cm^3 and a porosity ε = 0.38; for the Rainclean®, ρ = 1.79 g/cm^3 and ε = 0.56. Based on these initial estimates, the parametric analysis was carried out by testing all the combinations between the parameters presented in Table 3.

Table 3. Values used for the parametric analysis of the hydraulic parameters of the Richards model and the parameter n of the Manning-Strikler equation.

	K_s (m/s)	**θ_s (-)**	**α (1/m)**
Deposit	8.10^{-5} – $2.55.10^{-4}$ – 1.10^{-3} – $2.5.10^{-3}$	0.38 – 0.8	1 – 5 – 9
Sand	3.10^{-4} – 8.10^{-4} – 1.10^{-3} – $2.5.10^{-3}$	-	1 – 5 – 13 – 17

n Manning- Strikler (-)
0.01 – 0.025 – 0.05 – 0.075

The results obtained by simulation were compared with the data acquired on filter 1 (sand only) during a "dry weather" feeding batch in order to obtain the best match between the different water heights measured in situ (three different locations) and the flow rates measured at the outlet. Figure 5 shows the simulation results that best match the measured water levels and outflow

rates. The set of hydraulic parameters used to obtain these results is shown in Table 4. From the measured water level values, it is observed that, due to the length of the drains, pressures increase within it as previously shown (see The underdrain model section, Morvannou et al. (2023)). As a result, the water exits the drain towards the porous medium, leading to higher water levels in the filter downstream of the upstream piezometer. In the model, however, the direction of water flows entering the drain has been constrained: water can only enter the drain, not leave it. This is why the simulated outflows are higher (maximum flow = 19.3 L/s) than the observed flows (maximum flow = 10.2 L/s) and the measured water heights (max = 0.89, 0.71 and 0.64 m for the upstream piezometer, middle and downstream piezometers, respectively) are lower than those simulated for the middle and downstream piezometers (max = 0.32 and 0 m, respectively) and higher for the upstream piezometer (max = 0.78 m).

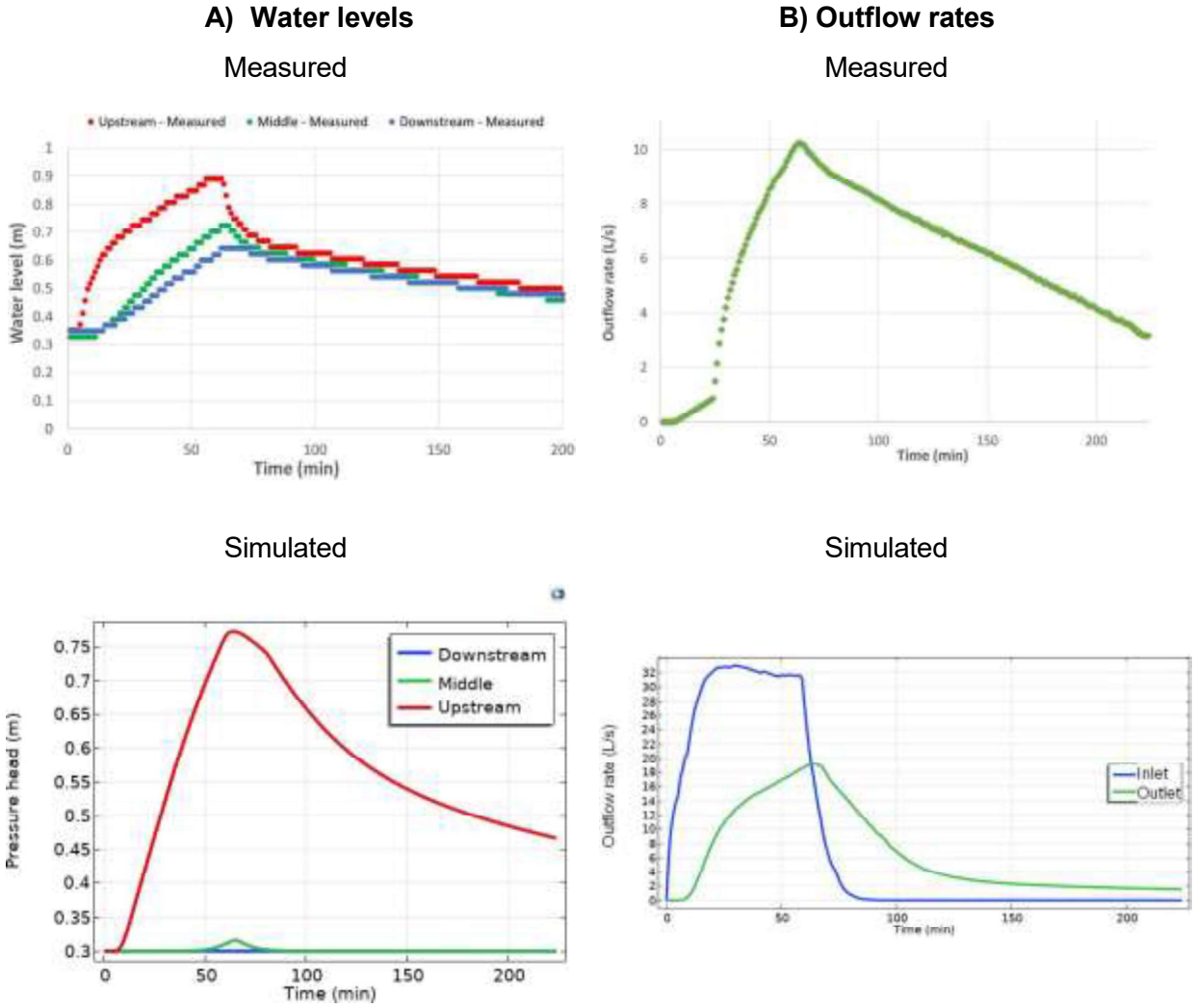

Figure 5: Evolution of water heights (A) and outflow rates (B) measured and simulated by the COMSOL Multiphysics model for a "dry weather" feeding batch for the hydraulic parameter set: n (Manning- Strikler) = 0.075, K_s filter = 2.5.10^{-3} m/s, α filter = 1 m^{-1}, K_s deposit = 2.5. 10^{-3} m/s, α deposit = 1 m^{-1}, θ_s deposit = 0.38

The hydraulic parameters of each layer are detailed in Table 4.

Table 4. Values used for the parametric analysis of the hydraulic parameters of the Richards model and the parameter n of the Manning-Strikler equation.

Layer	K_s (m/s)	θ_r (-)	θ_s (-)	α (1/m)	n (-)	l (-)	n Manning-Strikler (-)
Deposit	$2.5.10^{-3}$	0	0.38	5	2	0.5	0.075
Sand	$2.5.10^{-3}$	0	0.38	1	2	0.5	
Rainclean®	$1.89.10^{-3}$	0.2	0.56	5	2	0.5	
Drainage	10.10^{-3}	0	0.38	5	2	0.5	

2.5 The transport model

Transport of dilute species in porous media is governed by the advection-dispersion equation. This transport is simulated in the deposit, sand and Rainclean® layers. Dispersion, adsorption and desorption phenomena are considered for these three layers.

The values of the longitudinal dispersion coefficients determined during the simulations of the tracer tests carried out in task B3.1 for sand and Rainclean® are $2.74.10^{-6}$ m^2/s and $4.62.10^{-6}$ m^2/s, respectively. For the deposit, the same value as for the Rainclean® was considered. Dispersion is considered to be asymmetrical between longitudinal and transverse dispersion. In fact, the transverse dispersion is much smaller than the longitudinal dispersion by about one to two orders of magnitude (Bear, 1972). It is generally set at a value of 1/10 of the value of the longitudinal dispersion (Domenico and Schwartz, 1990; Appelo and Postma, 1996). In this study, the values of the transverse dispersion coefficients are thus defined as $2.74.10^{-7}$ m^2/s and $4.62.10^{-7}$ m^2/s for sand, Rainclean® and deposit, respectively.

With regard to the adsorption and desorption of micropollutants, the kinetics of these phenomena are not taken into account, i.e. adsorption and desorption are instantaneous.

The diluted species considered

The first species considered for the simulations is amino-G acid, in order to reproduce its behavior in the filters observed during tracer tests (see Tracer test experiments on the Bugeaud treatment wetlands section hereafter). Once its behavior has been reproduced and validated, the transport model can be used to simulate the fate of the micropollutants.

The metallic micropollutants selected for the simulations are: Cadmium (Cd), Copper (Cu), Nickel (Ni), Lead (Pb) and Zinc (Zn). The organic micropollutants selected for the simulations are: 4-nonylphenol (NP), 4-tert-octylphenol (OP) and Bisphenol-A (BPA).

To simulate the adsorption and desorption processes, it is necessary to know the parameter values of the adsorption isotherms for the amino-G acid and the micropollutants selected. These values were determined for Rainclean® either by batch or by inverse modelling in task B3.1.

The parameter values of the adsorption isotherms for the amino-G acid and the micropollutants were not determined for the deposit. Therefore, the following rule was applied: the parameter values of the adsorption isotherms determined for the Rainclean® for metallic and organic micropollutants were divided by 10 and 5, respectively, according to the supposed greater affinity of the organic micropollutants than the metallic micropollutants with the deposit. For the amino-G acid, the global adsorption efficiency was divided by 10.

For sand, the parameter values of the adsorption isotherms for the micropollutants used for the simulations are those determined by batch in task B3.1, with the exception of Cd and Ni, for which the batch values for sand were higher than those for sediment. Thus, for these two metals, the parameter values of the adsorption isotherms determined for the Rainclean® were divided by 100.

Table 5 shows the parameter values of the adsorption isotherms used in the simulations for Rainclean®, the deposit and the sand corresponding to the amino-G acid and/or the selected micropollutants.

Table 5. Parameter values for adsorption isotherms on Rainclean®, sediment and sand for G-amino acid and/or each micropollutant selected for the simulations.

DEPOSIT

Amino-G acid		20 cm
Isotherm		
Langmuir	qm [mg/g]	0.02
	K_L [L/mg]	0.422

Micropollutants

Isotherm		Cd	Cu	Ni	Pb	Zn	BPA	OP	NP
Linear	Kd [L/kg]	40.9		7.3	499.9			1778	2060
Langmuir	qm [µg/g]		1995			884	14		
	K_L [L/µg]		9.75E-05			5.72E-04	0.204		

RAINCLEAN®

Amino-G acid		20 cm
Isotherm		
Langmuir	qm [mg/g]	0.02
	K_L [L/mg]	4.22

Micropollutants

Isotherm		Cd	Cu	Ni	Pb	Zn	BPA	OP	NP
Linear	Kd [L/kg]	409		73	4999			8890	10298
Langmuir	qm [µg/g]		1995			884	14		
	K_L [L/µg]		9.75E-04			5.72E-03	1.02		

SAND

Isotherm		Cd	Cu	Ni	Pb	Zn	BPA	OP	NP
Linear	Kd [L/kg]	4.09	110	0.73	69.4	43	13	42	70

3 Comparison with tracer test experiments

3.1 Tracer test experiments on the Bugeaud treatment wetlands

3.1.1 Tracer test under "Dry weather" operating mode

A tracer test has been performed in this operation mode for filter 1 only. In a tracer test, a known amount of a chemical known to resist degradation is added to a batch, hereafter referred to as the tracer batch. The concentration of the tracer is measured and recorded continuously at the outlet of the filter over the course of several days using a fluorimeter.

Dry weather tracer test has been performed once the maximum level of the dry weather operating mode has been reached in the pumping station (120 m^3). The aim of this tracer test is to evaluate how water flows within filter 1 (residence time, type of flow) and if preferential flows and/or dead zone exist when the filter is fed according to the dry weather operating mode.

The theoretical residence time[2] is estimated to 2 hours during the "dry weather" operating mode. The tracer that was selected for this experiment is amino-G acid (7-aminonaphtalène-1,3-disulfonic acid).

Prior to the initiation of the experiment, the fluorimeter utilized for the monitoring of tracer concentration at the filter outlet underwent calibration. This calibration was conducted using water samples collected on November 2, 2022, at the outlet of the filter (following a period of three days with no precipitation). The water samples were then mixed with known quantities of amino-G acid, thereby creating a solution with tracer concentrations ranging from 0 ppb to 1,000 ppb. The calibration curve that resulted from the aforementioned process is expressed by the following equation: $C_{outlet} = 4.4685 \times V_{fluorimeter} - 16.557$, where C_{outlet} is the concentration in amino-G acid and $V_{fluorimeter}$ is the voltage observed by the fluorimeter.

150.04 g of amino-G acid were waited before the experiment and kept into a dry container before being mixed with the influent. Table 6 summarizes the main data on the tracer test performed under "dry weather" operating mode.

Table 6. Summary of the characteristics of the "dry weather" operating mode tracer test

		Dry weather operating mode
Amino-G acid mass	g	150.04
Volume of the batch (m^3)	m^3	120
Number of batch per day	-	6.5
Inlet tracer concentration	g/m^3 / ppb	1.3 / 1255
Batch flow rate	L/s	33.6
Duration of the tracer batch	min	59
Estimated volume of filter impacted by the flow	m^3	72

The optical measurement cell of the fluorimeter was placed vertically inside the standpipe so that it is always in water (Figure 6). The monitoring time step was set to one minute, and the recording commenced 10 minutes prior to the tracer batch. This approach was taken to measure the line base (without tracer).

[2] The theoretical residence time is estimated by dividing the volume of the pore space of the saturated layer of the filter by the inflow rate.

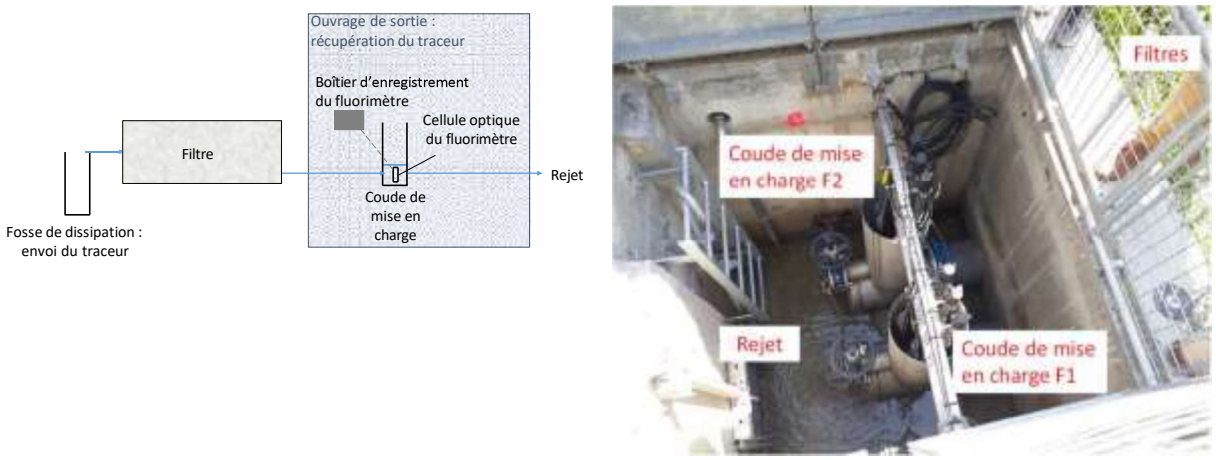

Figure 6. Sketch of the experimental setup at the outlet (left) and picture (right)

In addition to the pressure probe permanently installed in the standpipe and another one was added by Cerema in order to have recording at the same time step than the fluorimeter. Using Equation 2, the flow rate at the outlet was therefore estimated every minute.

3.1.1.1 Startup of the tracer test

Filter inlet: Prior to the initiation of the pumping process, the amino-G acid powder was diluted with water in a 15-liter bucket using water collected from the dissipation pit. In light of the site's layout and the implemented access restrictions, the tracer was meticulously introduced onto the filter surface at the precise point of water arrival (Figure 7). The tracer was incorporated using a peristatic pump during the entirety of the tracer batch.

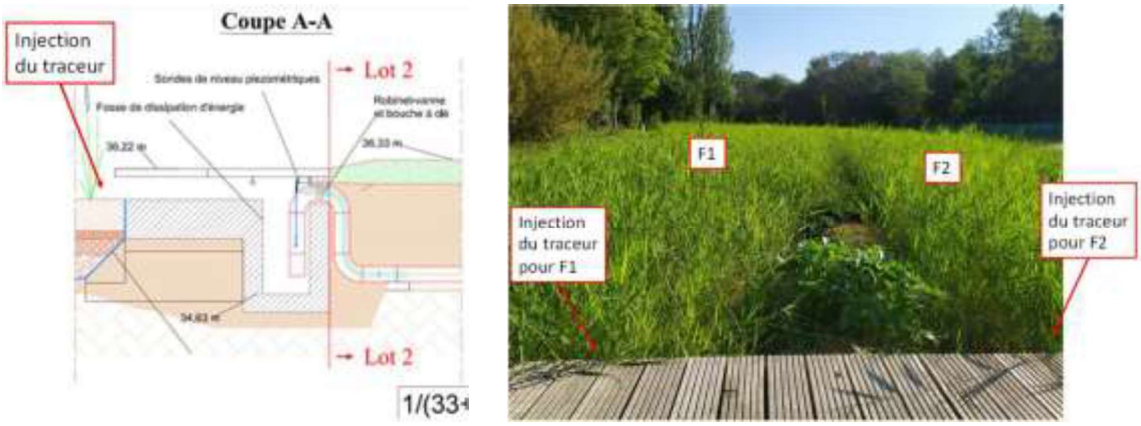

Figure 7. Blueprint and picture of the filter inlet where the tracer was injected.

The outlet flow rate and the fluorimeter voltage were monitored during 4 days with nor rainfall observed during this time.

3.1.1.2 Post-processing tracer test results

Breakthrough curve. Fluorimeter voltage values obtained during the tracer test were transformed into amino-G acid concentration using the calibration curve priory estimated. Figure

8 illustrates the evolution of the amino-G acid concentration at the outlet, as well as its recovery rate (i.e., the ratio of the mass of tracer recovered over the mass of tracer injected) over time.

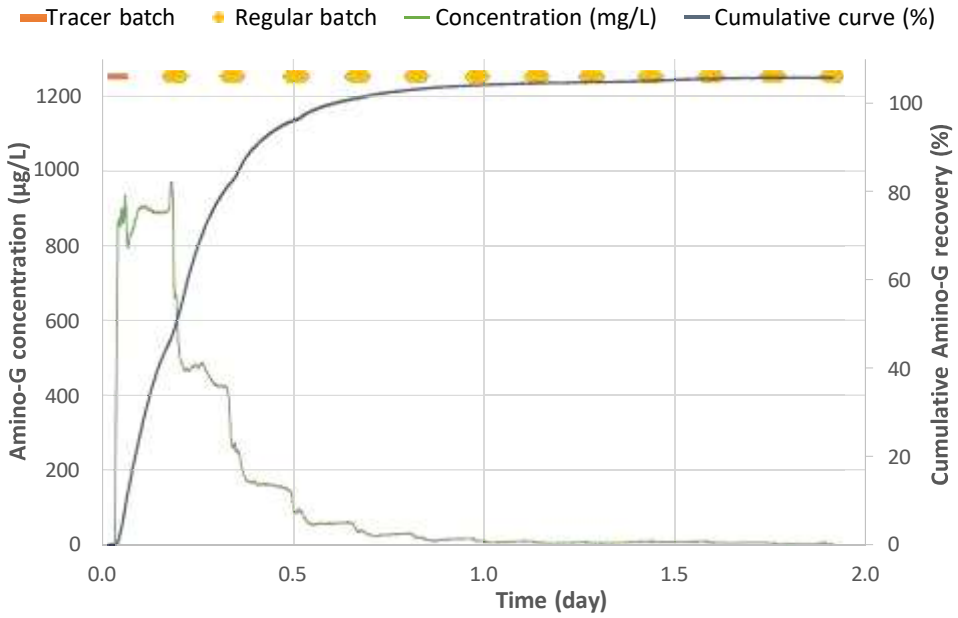

Figure 8. Amino-G acid concentration and recovery rate versus time at the outlet of the filter 1 during the tracer test performed under the "dry weather" condition

The final recovery rate was found to be approximately 106% (Figure 8). The observed value exceeds 100% and can be attributed to two primary factors. Firstly, calibration uncertainties contribute to this discrepancy. Secondly, uncertainties associated with measuring water flow also play a role. This finding indicates that the tracer was almost completely recovered, with minimal residual entrapping occurring due to dead zones or adsorption.

The concentration of the tracer increased at the outlet no later than during the first batch (i.e., 23 minutes after the beginning of the tracer batch, which had a total duration of 59 minutes). Furthermore, 67 g (i.e., 44.7% of the mass injected) of the tracer was recovered at the outlet by the end of the tracer batch. This result does not align with observations done on other system with a saturated layer. Indeed, it is expected that it will act as a buffer delaying the onset of the tracer by a period of several hours. Therefore, in the event that filter 1 is operated in dry weather mode, the early tracer outbreak signifies the existence of a hydraulic shortcut. In addition, the dilution effect associated with the saturated layer is minimal. The measured concentrations at the outlet were as high as 0.94 g/m³ when the inlet concentration was 1.26 g/m³. The volume of the saturated zone that is effectively affected by the tracer is estimated to be 41 m³, which constitutes 56% of the saturated area. This estimation is based on the peak concentration of the tracer. Consequently, dead volumes are present within filter 1 when operated in "dry weather" mode.

Moreover, 50% of the total mass of the tracer is recovered at the outlet after 4.2 hours, i.e., 35 minutes after the initiation of the second batch. It is evident that, at the conclusion of the second batch, a total of 121 g of the tracer (representing 80.4% of the injected mass) has been successfully recovered. The maximum concentration at the outlet is observed during the second batch, with a recorded value of 0.97 g/m^3. The mean residence time, as determined by the tracer test, is estimated to be 5.6 hours. This value exceeds the theoretical residence time estimate that is based solely on the saturated layer. Upon consideration of the preferential paths, it could be hypothesized that the observed residence time is less than the theoretical one. However, this is

negated by the subsequent neglect of the unsaturated zone, which plays an instrumental role in solute transfer.

Water levels. When the filter is operated under dry weather mode, water spreads onto the surface of the filter notably due to the formation of a deposit layer over the filtration layer. Figure 9 represents the part of the filter where surface flow has been observed when operating under “dry weather” condition. This phenomenon extends to approximately one-third of the filter surface.

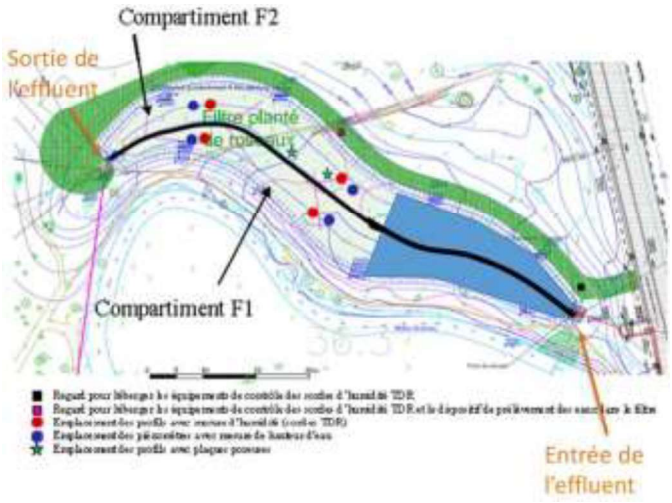

Figure 9. Bird view of both filters indicating in blue the area affected by surface flow when operated under "dry weather" mode

The "dry weather" operating mode was designed to prevent the re-mobilization of micropollutants following a rain event. The hypothesis posits that micropollutants are adsorbed within the filtering layers, specifically the unsaturated zone. Therefore, during the "dry weather" operating mode, water will only flow through a small fraction of the unsaturated zone. This is achieved by applying small but frequent batches. However, the tracer test showed that the applied volume (120 m³) exceeded the originally planned volume (50 m³) by more than a factor of 2. In addition, a surface deposit several centimeters thick was observed over half of the filter surface, which facilitated the dispersion of the water beyond the inlet point.

As a result, the filter volume affected by the passage of water in dry weather is much greater. Figure 10 shows the evolution of water height values measured at various points ("Upstream", "Middle", "Downstream") of filter 1 and at the outlet during tracer test. These figures enable us to estimate the area affected by the spreading of water during dry weather.

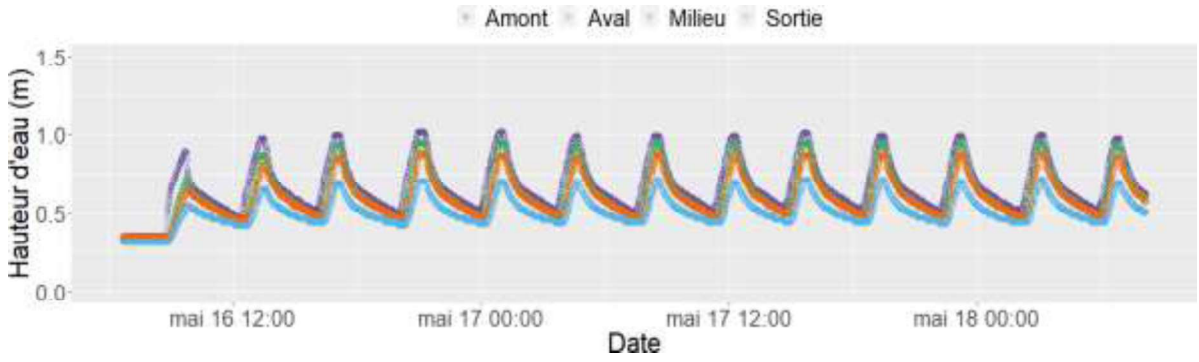

Figure 10.Evolution of water heights measured in filter 1 and at the outlet during tracer test

When filter 1 is fed during dry weather tracer test, **water levels increase at all measurement locations** (**Erreur ! Source du renvoi introuvable.**). On the other hand, there is also a **discrepancy** between the "Upstream", "Middle", "Downstream" and "Outflow" water level values. For each batch, the maximum water heights measured are systematically highest at the "Upstream" measurement point, then decrease with distance from the feed point, ending with the lowest maximum values measured at the filter outlet.

In addition, the water level values do not increase at the same time; there is a **time lag between the launch of a batch and the increase in water level values between the different locations** once a batch has been applied. Indeed, for a time T_0 being the launch of a batch in "dry weather", the water height increases by 10 ± 2 minutes, 20 ± 4 minutes and 26 ± 5 minutes at the "Upstream", "Middle" and "Downstream" locations, respectively. Once the water has reached the "Downstream" location, it takes an average of 3 ± 2 minutes for the water height at the filter outlet to increase. Prior to the start of tracer test, filter 2 was fed. The tracer batch was applied after a 10-day rest period. After a rest period, the time required for the water to reach the "Upstream", "Middle", "Downstream" locations and the outlet of filter 1 during the first application was 4 minutes, 11 minutes, 12 minutes and 14 minutes, respectively. Thereafter, the time taken for the water to reach the "Upstream", "Middle", "Downstream" and "Filter 1" locations increases with each successive application. For the 13th batch (last batch of tracer test), the time required for water to reach the "Upstream", "Middle", "Downstream" and "Filter 1" locations during the first batch is 14 minutes, 25 minutes, 30 minutes and 34 minutes, respectively.

On the other hand, once the tracer batch has been applied, the water depth values never drop below 35 cm for the three filter locations until the end of the tracer test process. During the tracer batch application, the 20 cm depth is only reached for the "Upstream" location, then this depth is reached for all subsequent batches for this location. The 20 cm depth is reached for the "Middle" site from the second batch application until the end of the tracer test process, and the 20 cm depth is reached for the "Downstream" site from the fourth batch application on the filter. The 5 cm depth is never reached for the "Middle" and "Downstream" locations. They are reached for the "Upstream" site from the second batch to the end of the tracer test.

3.1.1.3 Hydraulic behavior of filter 1 in dry weather operating conditions

When steady state is reached (from the fourth batch onwards), the water brought in by the batches spreads as far as the "Upstream 1" and "Upstream 2" locations in the first few minutes (visual observation, as the values provided by the TDR probes do not allow this to be observed), and as far as the "Middle" location 54 ± 3 min after the batch is launched. The water infiltrates to the bottom of the filter (with a gradient from the filter inlet to the outlet) and once it reaches the bottom of the filter, it fills from the bottom to the top of the filter, reaching the surface at the "Upstream" location, and to a depth of 8 cm and 17 cm at the "Middle" and "Downstream" locations, respectively. At the surface, the water spreads out to at least the "Middle" location, without reaching the "Downstream" location.

Figure 11 shows a summary diagram of the hydraulic operation of filter 1 in "dry weather" mode, once steady-state operation has been reached (after the first three batches have been applied and the filter has rested for several days).

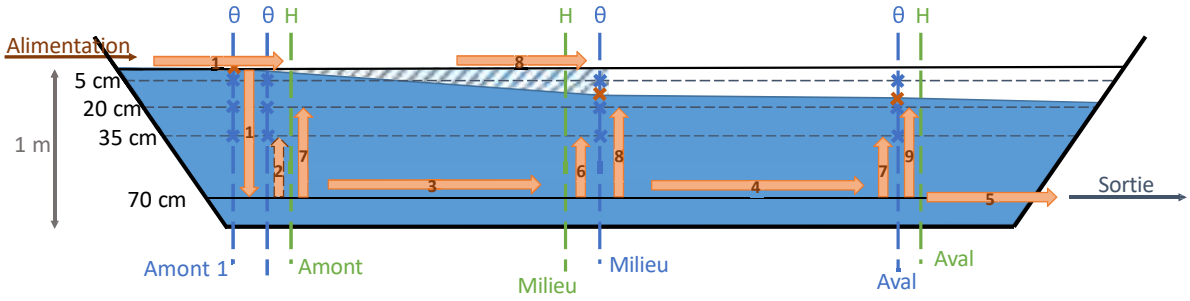

Figure 11. Summary diagram of hydraulic operation of filter 1 in dry weather

T_0 = Batch starts
T_1 = Rapid surface flow of water to "Upstream 1", "Upstream 2", "Upstream" (visual obs.) and infiltration
$T_2 = T_0 + 10 \pm 1$ min = Filling from bottom to top at "Upstream" location
$T_3 = T_0 + 21 \pm 2$ min = Water reaches the "Middle" location
$T_4 = T_0 + 28 \pm 3$ min = Water reaches the « downstream » location.
$T_5 = T_0 + 31 \pm 2$ min = Filter starts flowing out of the filter
$T_6 = T_0 + 38 \pm 3$ min = Filling from bottom to top to a depth of 35 cm in the "Middle" position
$T_7 = T_0 + 45 \pm 2$ min = Fill from bottom to top to a depth of 20 cm at the "Upstream" location and to a depth of 35 cm at the "Downstream" location.
$T_8 = T_0 + 55 \pm 2$ min = Filling from bottom to top to a depth of 20 cm at the "Middle" location and surface drainage to the "Middle" location
$T_9 = T_0 + 65 \pm 2$ min = Filling from bottom to top to a depth of 20 cm at the "Downstream" location

Tracer test was also carried out on filter 2 in "dry weather", but due to water overflows between the two filters at the water inlet, the data acquired cannot be used. In fact, some of the water and therefore the tracer sent to filter 2 passed through filter 1, making it impossible to carry out a mass balance and interpret the data.

3.1.2 Tracer test under “Rain weather” operating mode

The filter is fed in two stages during "rain weather". Firstly, the operating filter is fed at a flow rate of 70 L/s up to a so-called "high ponding" level (0.97 m and 1.06 m above the filter bottom for filters 1 and 2, respectively). Once this level is reached, the feed is stopped until the water level in the filter reaches a so-called "low ponding" level (0.93 m and 0.97 m relative to the filter bottom for filters 1 and 2, respectively). Once this level has been reached, the filter is fed again, at a flow rate of 40.1 L/s, up to the "high ponding" level. Here again, feed is stopped until the water level in the filter reaches a so-called "low ponding" level. The alternation between "high ponding" and "low ponding" levels continues until the "rain weather" operating mode is deactivated (when the level in the pumping station returns to the "pump stop level" (0 m3) or the "heavy rain" level (1000 m3) is exceeded).

Hydraulic tracer test was carried out in "rain weather" on filter 1 (sand only) at the Bugeaud site. It was carried out once steady-state conditions had been reached, i.e. once the first batch had been sent out and the maximum water level ("high ponding" level = 5 cm above the filter surface) had been reached. The tracer was injected when the second batch was sent to filter 1. This tracer test enables us to determine how the flow takes place in filter 1 (residence time, type of flow) and whether there are preferential passages (or not) and/or dead zones.

Theoretical hydraulic residence time is 3.8 hours for rain weather operating conditions for filter 1.

The tracer used for tracer test is, as for "dry weather" tracer test, amino-G acid (7-aminonaphthalene-1,3-disulfonic acid). Table 7 summarizes the main data on the tracer test performed under “dry weather” operating mode.

Table 7. Summary of the characteristics of the “rain weather” operating mode tracer test

		Rain weather operating mode
Amino-G acid mass	g	150.04
Volume of the batch (m^3)	m^3	51
Number of batch per day	-	31
Inlet tracer concentration	g/m^3 / ppb	2.9 / 2964
Batch flow rate	L/s	40.1
Duration of the tracer batch	min	21
Estimated volume of filter impacted by the flow	m^3	270

Breakthrough curve. Signal data (mV) obtained during tracer test were converted to amino-G acid concentration (ppb) using the equation established during fluorometer calibration. Figure 12 shows the evolution of the amino-G concentration measured at the outlet of filter 1, as well as its recovery rate when traced in "rain weather" operating mode.

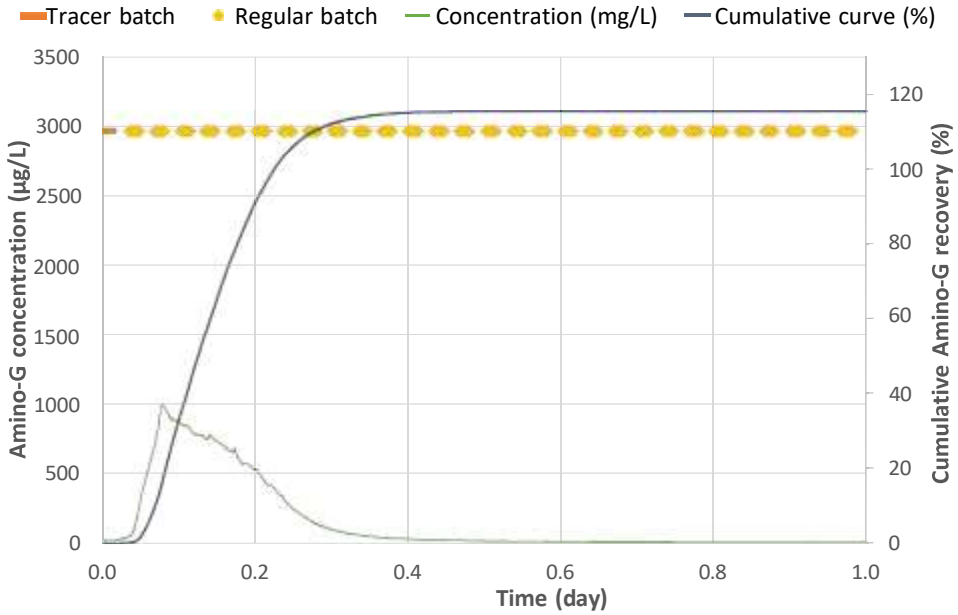

Figure 12 Amino-G acid concentration and recovery rate measured at the outlet of filter 1 during "rain weather" operating condition tracer test

Tracer recovery at the end of tracer test is around 115°% (Figure 12). The fact that the mass of tracer recovered at the outlet is greater than the mass of tracer applied at the filter inlet is certainly due to the uncertainties associated with the flow values calculated at the filter outlet. Nevertheless, this recovery rate is considered acceptable (tracer recovery rate between 80°%

and 120°%) for describing and interpreting the hydraulic operation of filter 1 during rain weather operating conditions.

4 Simulation of tracer tests on the two filters

Simulations were carried out under the same conditions as those applied during the tracer tests (Table 6 and Table 7) in order to simulate the behavior of the amino-G acid in the filters during the 'dry weather' and 'rain weather' modes. and to see where this species is stored or not and which parts of the filters are more or less It is also possible to determine which parts of the filters are more or less stressed and to see where this the amino-G acid is stored or not. As the tracer tests were only carried out on filter 1, without Rainclean®, the results of the simulations of filter 2 cannot be compared with any measurements of amino-G acid concentrations at the outlet.

4.1.1 Model settings

The hydraulic parameters taken into account were those shown in Table 4. For filter 1 (sand only), no adsorption was simulated, whereas the adsorption parameters shown in Table 5 were taken into account for the Rainclean® layer and the deposit for filter 2.

Filters were considered to be saturated over the first 30 centimeters of the drainage layer and considered to be clear of amino-G acid.

The characteristics of the simulated 'dry weather' and 'rain weather' batches are presented in Table 8. Two days of tracer test were simulated for each filter, for both 'dry weather' and 'rain weather' modes.

Table 8. Characteristics of 'dry weather' and 'rain weather' batches.

Dry weather – Number of batches/day = 6					
Feeding				Rest	
Duration (min)	Water flow (L/s)			Duration (min)	
59	33.6			165	

Rain weather – Number of batches/day = 18					
Feeding				Rest	
Filling		Maintain level		Filling	Maintain level
Duration (min)	Water flow (L/s)	Duration (min)	Water flow (L/s)	Duration (min)	Duration (min)
64	72	22	40.1	46	26

4.1.2 Results

A series of numerical experiments were conducted, employing identical operating conditions to those observed during tracer tests. Furthermore, a numerical experiment was conducted to simulate a tracer test during rain weather operating mode, under the assumption that the tracer had been added once the entire surface of the filter had been flooded. The results of these

simulations are presented in Figure 13. A comparison of the simulation results of the tracer test conducted under dry weather operating conditions on filter 1 with the experimental findings reveals that the numerical model accurately replicates the curve's shape. The main peak occurs four hours after the initiation of the batch, whereas during the experiment, the peak was measured 4.6 hours prior. Nonetheless, the model proved incapable of predicting the peak concentration, which was found to be only half of the value that was observed during the course of the experiment. The discrepancy can be attributed to (i) the omission of certain transport mechanisms (like dual-porosity preferential flows) from the numerical model and (ii) mass-balance errors that despite all the efforts of the modelers have remained significant probably due to the complexity of the coupling at the outlet boundary. The same conclusions can be drawn when comparing the results of the tracer experiments and numerical experiments for filter 1 under rain weather operating conditions.

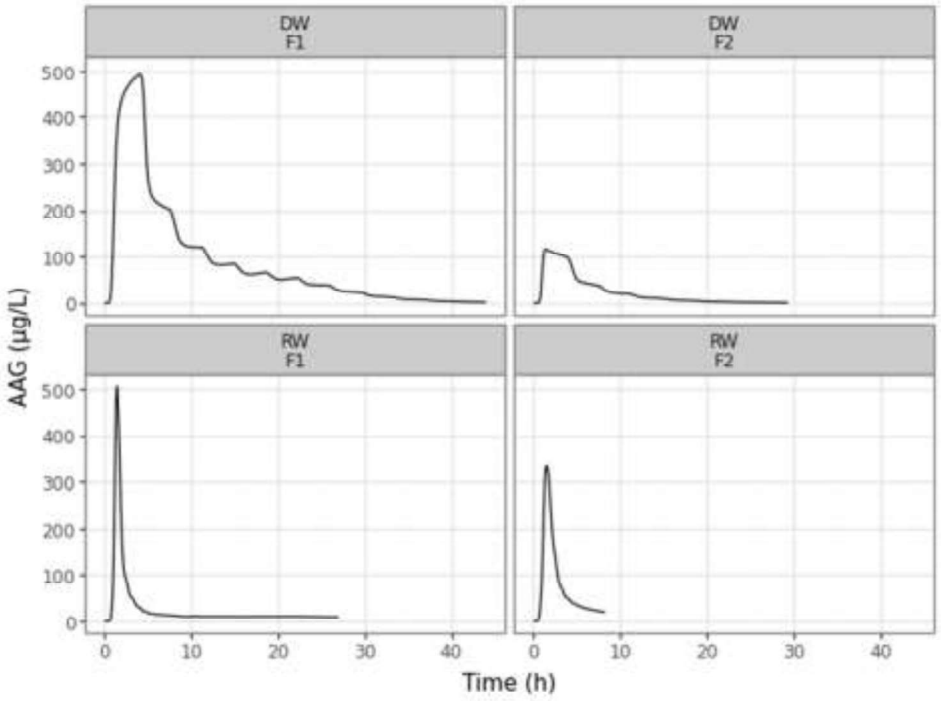

Figure 13. Tracer breakthrough curves simulated by the numerical model for both filters (F1 and F2) and both operating modes (DW: dry weather and RW: rain weather)

A significant input of the numerical experiments are the results obtained for filter 2 for no experimental tracer test has been performed. The incorporation of the adsorption process leads to a substantial modification in the shape of the breakthrough curve under the "dry weather" operating mode, with a considerable portion of the tracer being retained within the filtering media. The peak concentration undergoes a reduction from 500 µg/L for filter 1 to 120 µg/L for filter 2. Nevertheless, the decline in the adsorption capacity of filter 2, as indicated by the "wet weather" simulation results, is less pronounced. This finding suggests that the operating mode may not be optimal for adsorption, as predicted by the numerical model. Finally, it should be noted that the results of the simulation of filter 2 under wet weather operating conditions end before less than 10 hours of simulation while the simulation time has been set to 30 hours. This is the consequence of the failure of the non-linear solver to converge.

Numerical results provide additionally the distribution of the tracer within the filter media during the simulation. This is a very valuable piece of information since the suboptimal distribution of the influent as been identified as a potential weakness of the filter design.

Figure 14 and Figure 15 show the evolution of the distribution of the concentration of amino-G acid in solution for ‘dry weather‘ (A) and ‘rain weather‘ (B) modes in filter 1 and 2, respectively, at different simulation times of the tracer experiments.

For the filter 1 operating under dry weather conditions, it is observed that the tracer remains in the first half of the filter. The tracer that remains in the filter after the first batch (T = 220 min) is progressively washed out during the subsequent batch (T = 270 min) but does not spread downstream. At time T = 660 min, a residual concentration is observed upstream in the fraction of the filter that does not have drainage network. This is a potential dead zone in dry weather operation mode , which confirms what was observed during the tracer on filter 1.

For the filter 1 operating under wet weather conditions, tracer patterns differ. After the first batch, the tracer is evenly distributed over the filter surface and reaches quickly the drainage network. The path that the tracer takes is strongly influenced by the hydraulic limitations associated to the underdrain network. It is observed that at time T = 135 min, the tracer flows towards a section of the underdrain network located just upstream of the junction of the two antennas.

For filter 2, it is first important to state that the concentration displayed in figure 12 are the solute concentration and therefore do not picture the tracer entrapped in the Rainclean material (solid concentration). The patterns are more similar between dry and rain weather operating conditions that they are for filter 1. Higher concentrations are observed in the sand layer above the Rainclean all over the tracer test. This result is at first counter intuitive. We made the following assumption to explain this result: the concentration in the Rainclean is high because of the equilibrium with the solid concentration which corresponds to the tracer retained by adsorption. This creates a gradient that may enable diffusion upstream. Even if the latter is limited its impact on the concentration can be significant since the water content is low. The difference between dry and rain weather operating conditions is mainly due to the repartition of the tracer over the surface with the upstream section being less solicitated during rain weather operating condition than during dry weather operating conditions.

Three zones are distinguished for the two filters, whether in dry or rain weather mode: a dead zone, an active zone and a bypass zone. The dead zone is located at the beginning of the filters, where the water is brought in and where there is no drain to collect it. The active zone is located in the middle of the filters, starting where the drainage network begins and covering an area of one third of each filter. The bypassed zone is located downstream. The active zone is larger in rain weather than in dry weather. The presence of these three zones can play a positive or negative role in the retention and/or release of micropollutants.

Filter 1 (sand only)	
A) Dry weather	B) Rain weather
T = 220 min (3.7 h) – End of rest period after the tracer batch	T = 45 min (0.75 h) – End of rest period after the tracer batch
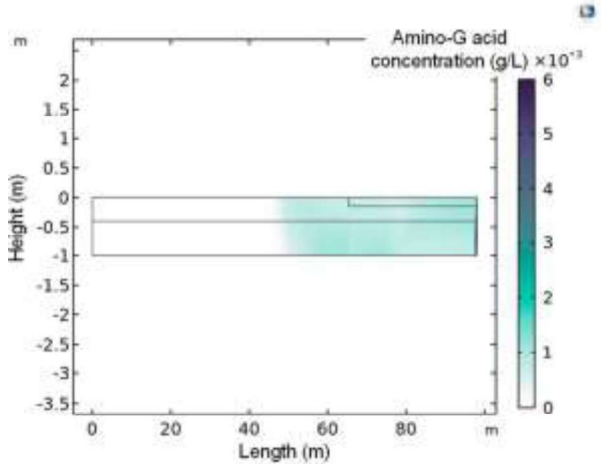	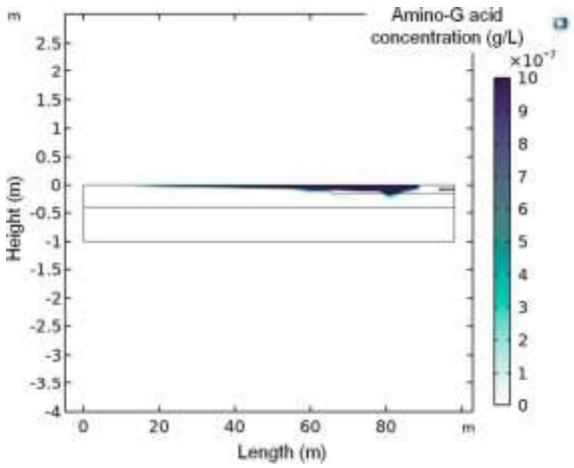
T = 270 min (4.5 h) – During the second batch (without tracer)	T = 135 min (2.25 h) – During the third batch (without tracer)
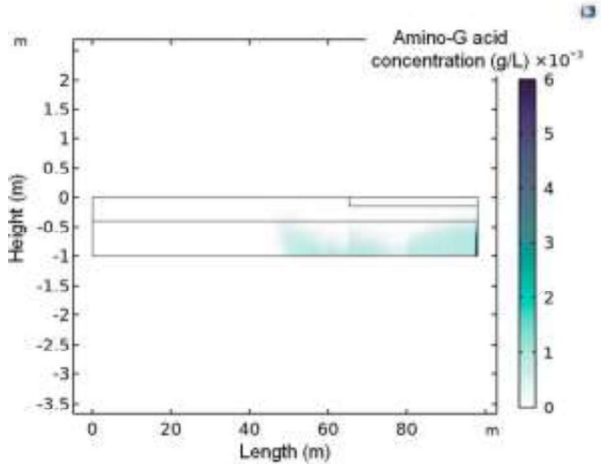	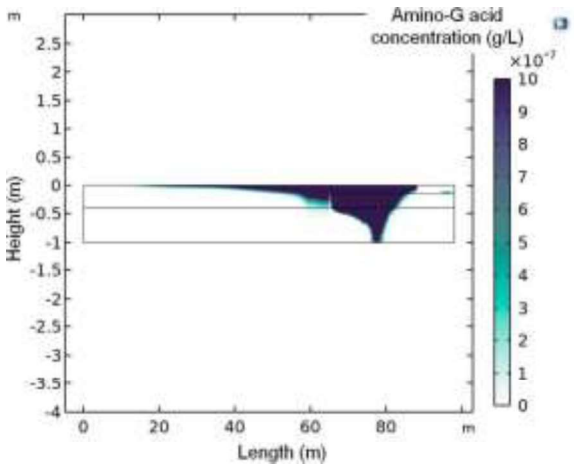
T = 660 min (11 h) – End of rest period after the third batch (without tracer)	T = 1620 min (27 h) – End of rest period after the thirty-sixth batch (without tracer) = end of tracer test
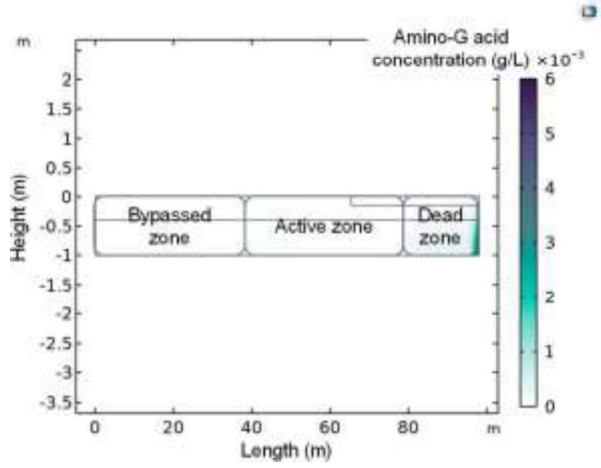	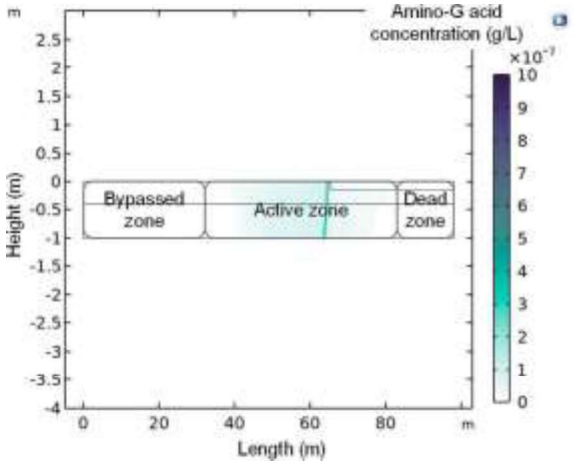

Figure 14: Evolution of the distribution of the amino-G acid concentration at different simulation times of the tracer test in filter 1 for 'dry weather' (A) and 'rain weather' (B) modes

Filter 2 (Rainclean®)	
A) Dry weather	B) Rain weather
T = 220 min (3.7 h) – End of rest period after the tracer batch	T = 45 min (0.75 h) – End of rest period after the tracer batch
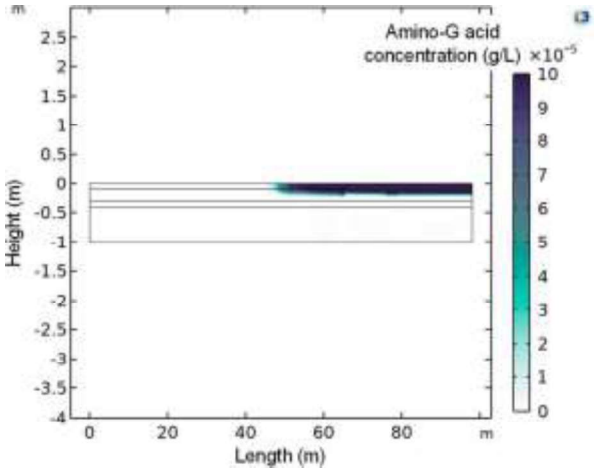	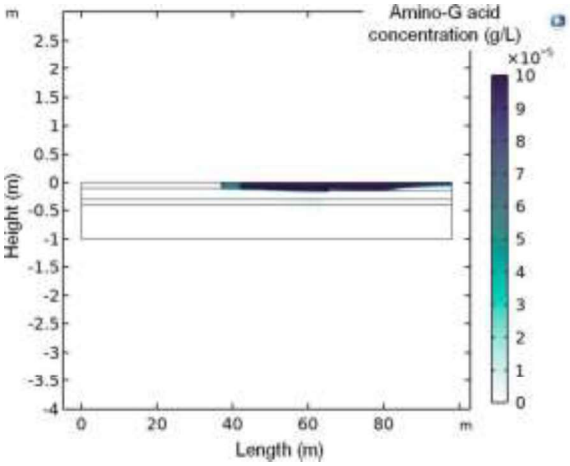
T = 270 min (4.5 h) – During the second batch (without tracer)	T = 315 min (5.25 h) – End of rest period after the seventh batch (without tracer)
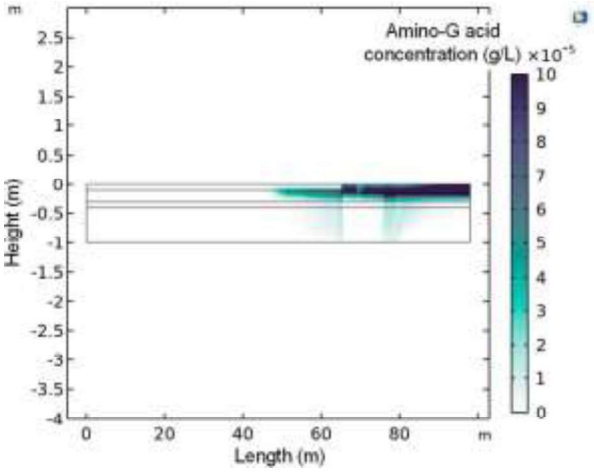	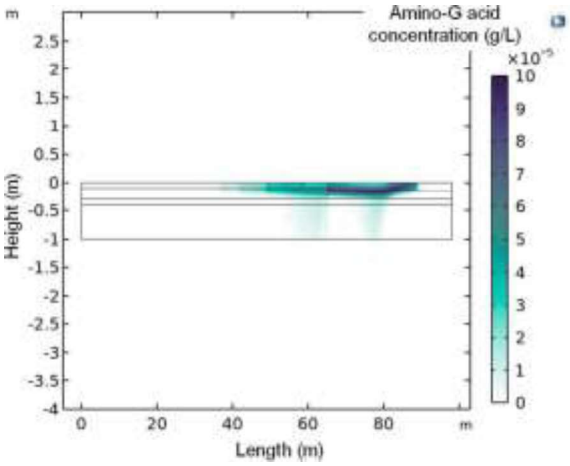
T = 660 min (11 h) – End of rest period after the third batch (without tracer)	T = 660 min (11 h) – End of rest period after the thirteenth batch (without tracer)
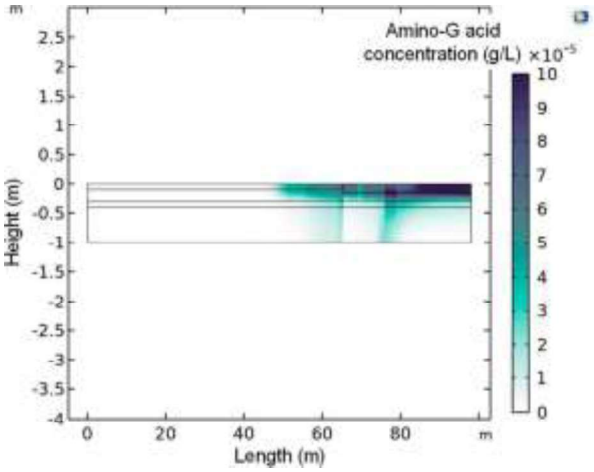	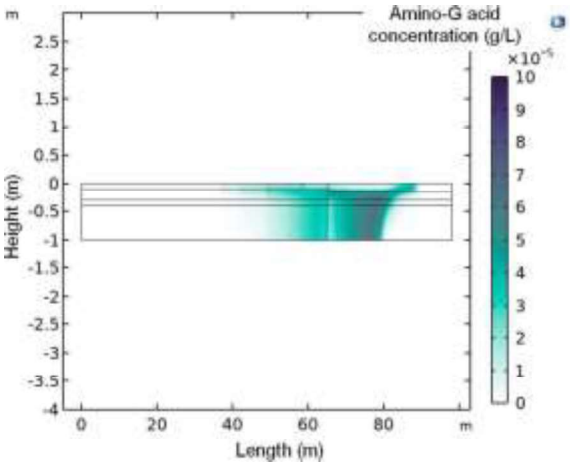

T = 2640 min (44 h) – End of rest period after the twelfth batch (without tracer) = end of tracer test

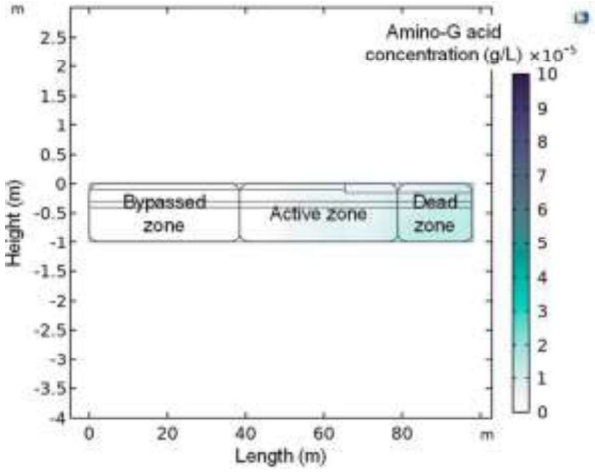

T = 1620 min (27 h) – End of rest period after the thirty-sixth batch (without tracer) = end of tracer test

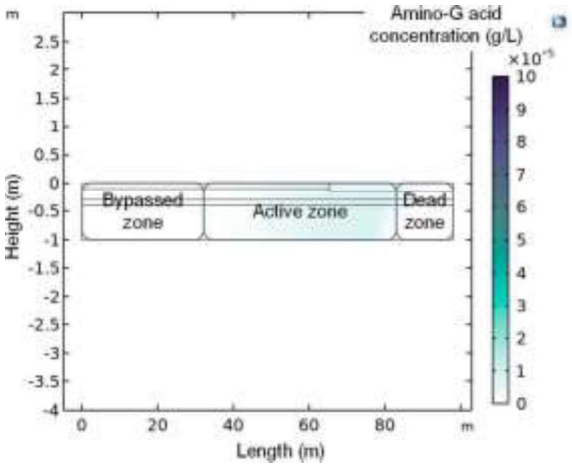

Figure 15: Evolution of the distribution of the amino-G acid concentration at different simulation times of the tracer test in filter 2 for 'dry weather' (A) and 'rain weather' (B) modes

When looking at the adsorbed quantities (Figure 16), it worth noticing that independently of the operating mode, most of the adsorption occurs in the first half of the filter. To estimate weather or not there are significant release of tracer after the tracer batch, the total mass of tracer accumulating in the filter has been estimated by integrating the adsorbed mass of filter domain (Figure 17). After oscillations during the two first batches, the value remain constant indicating no further leaching during the subsequent batches.

Filter 2 (Rainclean®)	
A) Dry weather	B) Rain weather
T = 220 min (3.7 h) – End of rest period after the tracer batch	T = 45 min (0.75 h) – End of rest period after the tracer batch
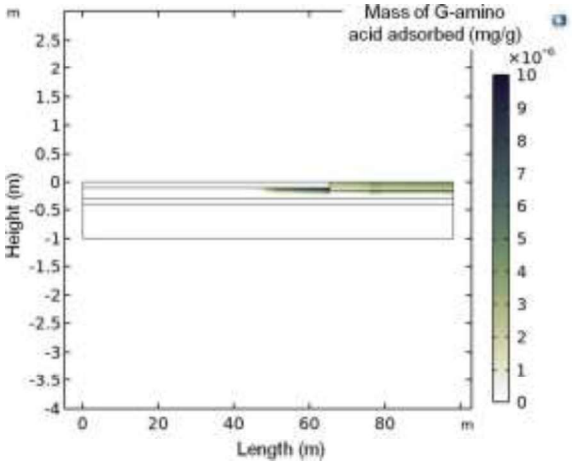	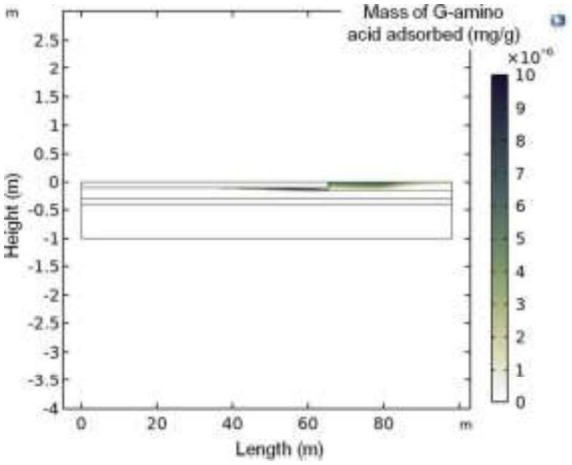
T = 440 min (7.3 h) – End of rest period after the second batch (without tracer)	T = 315 min (5.25 h) – End of rest period after the seventh batch (without tracer)
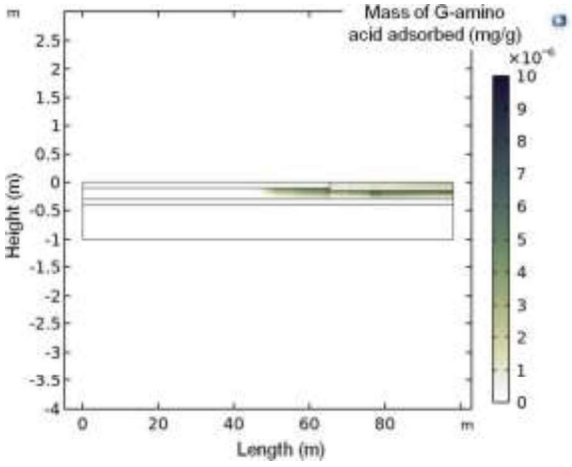	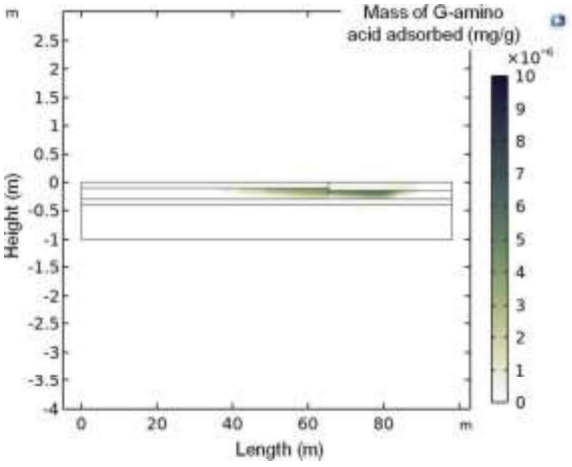
T = 660 min (11 h) – End of rest period after the third batch (without tracer)	T = 660 min (11 h) – End of rest period after the thirteenth batch (without tracer)
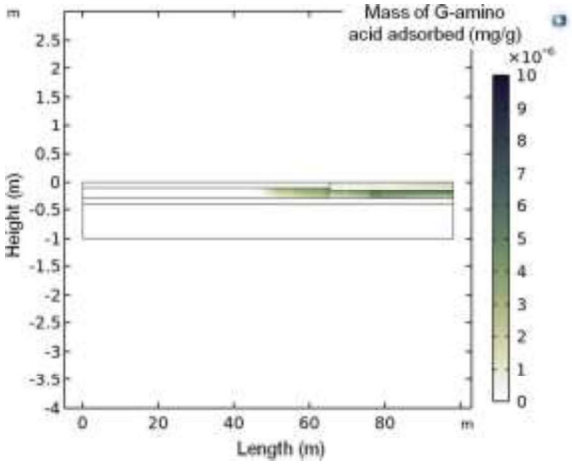	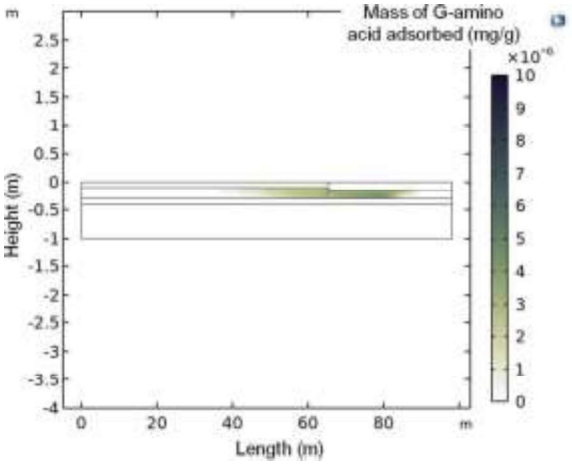

T = 2640 min (44 h) – End of rest period after the twelfth batch (without tracer) = end of tracer test

T = 1620 min (27 h) – End of rest period after the thirty-sixth batch (without tracer) = end of tracer test

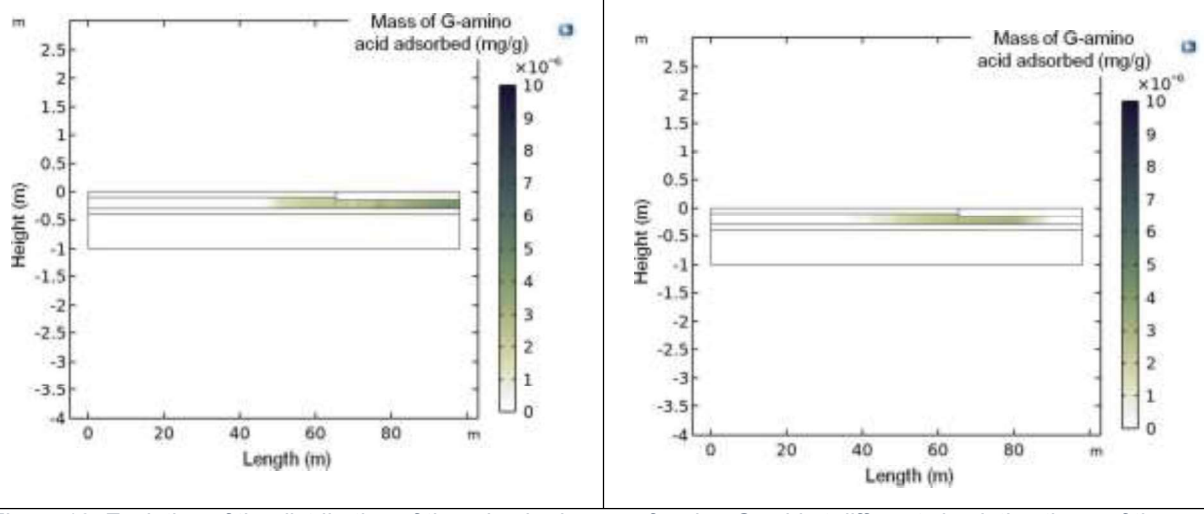

Figure 16: Evolution of the distribution of the adsorbed mass of amino-G acid at different simulation times of the tracer test in filter 2 for 'dry weather' (A) and 'rain weather' (B) modes

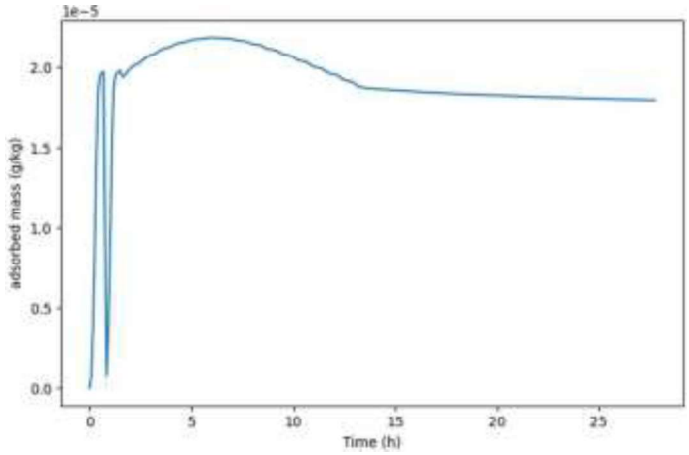

Figure 17. Total adsorbed mass on solid in the filter versus time

4.2 Simulation of a homogeneous distribution

An alternative scenario was tested by simulating the behavior of filter 2 (with Rainclean®) in 'dry weather' only, with another water distribution scenario. A uniform distribution of the tracer over the entire surface of the filter was applied in order to examine the potential impact of the water distribution system. This scenario was only applied to filter 2 because it is in this scenario that we are likely to see a difference with the current operation of the filter, since adsorption is simulated in this filter. Similarly, the work focused on 'dry weather', as it is this mode that would be the most different from uniform distribution, 'rain weather' being designed to have a rapid filling of the filter and, once filled, operating in a state closer to uniform distribution.

4.2.1 Model settings

The hydraulic parameters taken into account were those shown in Table 4. The adsorption parameters shown in Table 5 were taken into account for the Rainclean® layer and the deposit.

Filters were considered to be saturated over the first 30 centimeters of the drainage layer and considered to be clear of amino-G acid.

The characteristics of the simulated 'dry weather' batches are presented in Table 6. Two days of tracer test were simulated.

4.2.2 Results

Figure 18 shows the evolution of the distribution of the concentration of amino-G acid in solution (A) and the adsorbed mass (B) at different simulation times of the tracer test in filter 2 for "dry weather" mode. When the distribution of water on the surface of the filter is homogeneous, the entire surface of the filter is active. In addition, once the tracer has been applied to the entire surface, after the next batch application without tracer (T = 440 min (7.3 h)), the concentration in the filter is not homogeneous. A gradient is created and the concentration of amino-G acid in solution is greater towards the downstream end of the filter. It is at this point that the tracer leaves the filter well before the upstream end. This is because, as shown previously (The underdrain model), the smaller the distance between the slots in the drainage network and the outlet, the greater the pressure losses and consequently the greater the flows through the slots. Thus, even if the application of the water and tracer is homogeneous over the entire surface of the filter, the flows entering the slots in the drains are not homogeneous and the downstream part of the filter is more active than the upstream part. As a result, a zone at the inlet is always less involved in the transport of G-amino acid, as was seen during the tracer test simulations.

The mass of amino-G acid adsorbed is homogeneous during the first batches (see Figure 18: T = 45 min (0.75 h) - End of rest period after the tracer batch). Then over time, as the flow of tracer-free water is greater downstream of the filter, the desorption of amino-G acid is greater in this part (see Figure 18: T = 315 min (5.25 h) - End of rest period after the seventh batch) and a greater quantity remains adsorbed at the inlet at the end of the simulation (see Figure 18: T = 660 min (11 h) - End of rest period after the thirteenth batch).

A homogeneous supply of water to be treated containing contaminants would enable the entire surface of the filter to be used and would reduce the presence of dead zones. A properly sized and positioned drainage network goes hand in hand with this homogeneous water supply to obtain homogeneous flows and limit preferential flows inside the filter.

Filter 2 (Rainclean®) – Dry weather	
A) Amino-G acid concentration	B) Amino-G acid adsorbed
T = 220 min (3.7 h) – End of rest period after the tracer batch	T = 45 min (0.75 h) – End of rest period after the tracer batch
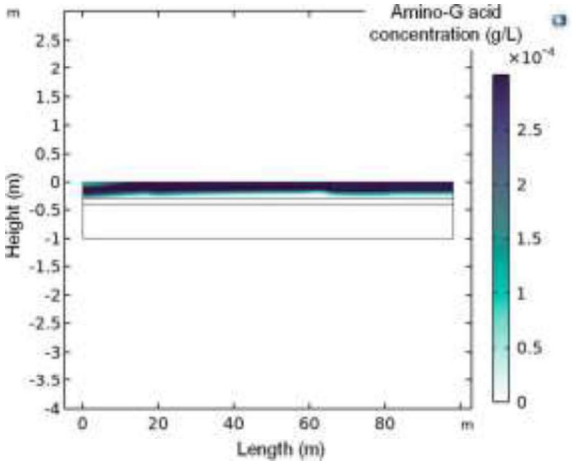	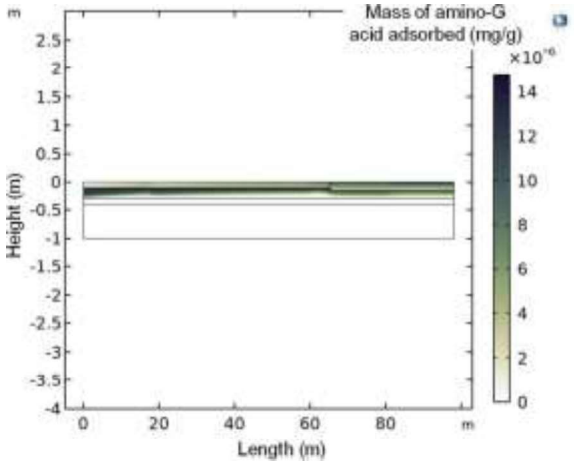
T = 440 min (7.3 h) – End of rest period after the second batch (without tracer)	T = 315 min (5.25 h) – End of rest period after the seventh batch (without tracer)
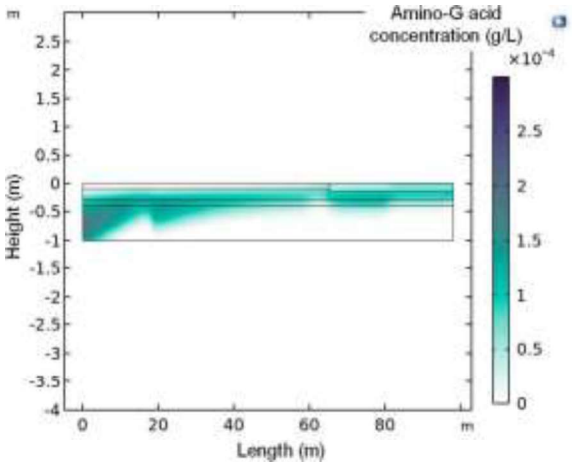	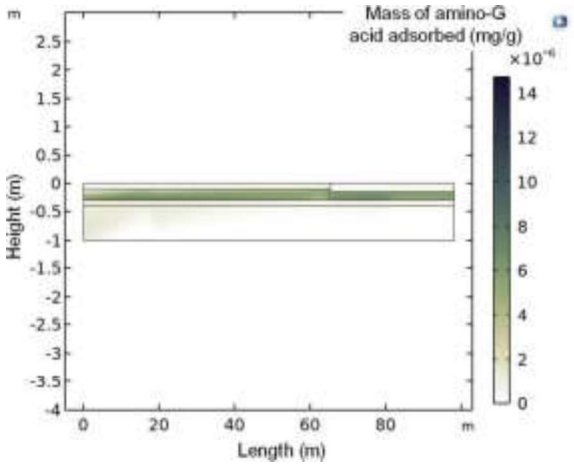
T = 660 min (11 h) – End of rest period after the third batch (without tracer)	T = 660 min (11 h) – End of rest period after the thirteenth batch (without tracer)
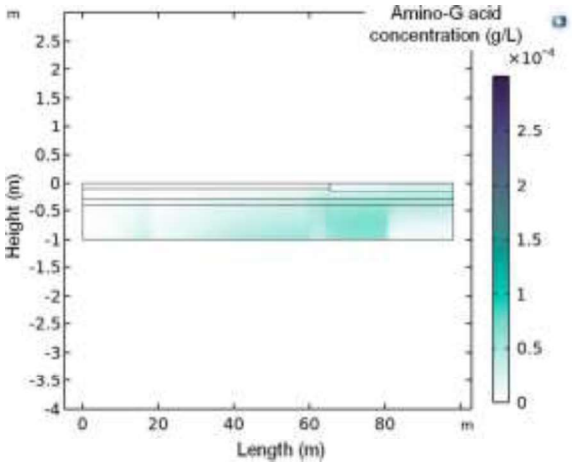	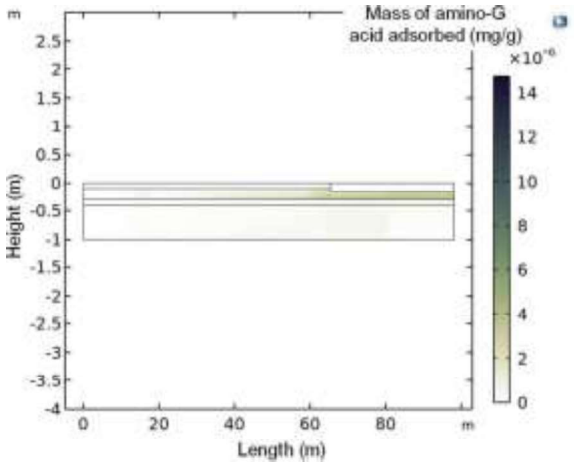

Figure 18: Evolution of the distribution of the concentration (A) and adsorbed mass (B) of amino-G acid at different simulation times of the tracer test in filter 2 for 'dry weather' mode

5 Dynamic simulations and the trajectory of micropollutants

5.1 At the beginning of treatment wetland operation

This scenario involves simulating a succession of 'dry weather' and 'rain weather' days, such as: one day of 'dry weather' followed by one day of 'rain weather' followed by one day of 'dry weather' then two days of 'rain weather' and finally returning to one day of 'dry weather'. Only the filter containing Rainclean® (filter 2) was involved to assess the behavior of micropollutants during these alternating periods of 'dry weather' and 'rain weather'.

5.1.1 Initial conditions for hydraulic and transport models

One simulation corresponded to one day. So, for the first simulation, the filter was considered to be saturated over the first 30 centimeters of the drainage layer and considered to be clear of any micropollutants. For each subsequent simulation, the initial condition was the state of the filter at the end of the previous simulation.

5.1.2 Water and micropollutant inputs

The characteristics of the simulated 'dry weather' and 'rain weather' batches are presented in Table 8. Inflow rates applied to each filter were stable during each batch.

Only dissolved concentrations of micropollutants were simulated. Table 9 shows the concentrations of dissolved metallic and organic micropollutants selected for the 'dry weather' and 'rain weather' simulations at the filter inlet (Gromaire *et al.*, 2022). The concentrations of micropollutants in 'dry weather' were arbitrarily defined as 100 times lower than the concentrations in 'rain weather'. For each type of water, input concentrations were stable throughout the duration of each batch.

Table 9. Simulated concentrations of dissolved metallic and organic micropollutants at filter inlets for 'dry weather' and 'rain weather' modes.

Dry weather							
Metallic micropollutants					Organic micropollutants		
Cd	Cu	Ni	Pb	Zn	BPA	OP	NP
µg/L					ng/L		
0,0016	2,51	0,13	0,039	3,62	46.30	10,10	44,90

Rain weather							
Metallic micropollutants					Organic micropollutants		
Cd	Cu	Ni	Pb	Zn	BPA	OP	NP
µg/L					ng/L		
0,16	251	13	3.9	362	4630	1010	4490

5.1.3 Results

Figure 19 to Figure 26 show the changes in the distribution of the concentration in solution and the mass adsorbed in filter 2 for the micropollutants studied (Cd, Cu, Ni, Pb, Zn, BPA, OP and NP) during the simulations alternating between dry and rain weather days. Each pair of figures shows the state of the filter at the end of each day.

We see the effect of adsorption on the Rainclean® adsorbent material and on the deposit layer. This adsorbent material increases the retention efficiency of micropollutants in filter 2. It can be assumed that for filter 1, without Rainclean®, the adsorption of micropollutants would have been low, mainly on the deposit.

As in the simulations of the tracer tests with amino-G acid, the three zones - the dead zone (where the drainage network is absent), the active zone and the bypassed zone - are present for all the micropollutants (for Ni, the bypassed zone is less important than for the others).

For some micropollutants, the concentrations in solution simulated in filter 2 are very low and the quantity adsorbed increases over time. Cd, Cu, Pb, Zn and BPA are the micropollutants that are always retained. Pb, OP and NP behave in the same way (Figure 22, Figure 25, Figure 26). For these micropollutants, even if the adsorption is strong, the concentrations in rainy weather are too high for everything to be retained and their outlet concentration increases over time. Ni, the simulated micropollutant with the lowest adsorption, is the only micropollutant whose presence in solution covers almost the entire surface of the filter. Moreover, because of its low affinity with Rainclean®, Ni accumulates in the dead zone at the filter inlet during each period of rain weather.

We can distinguish between alternating days of dry weather and rainy weather. There is clearly adsorption when the incoming water is more loaded during rainy weather, whereas there is desorption of elements previously adsorbed during dry weather because the incoming water is less concentrated. This is clearly seen in the case of Ni (Figure 21) at the end of a day of dry weather (day 3), where the quantity of Ni adsorbed in the first third of the filter is virtually zero, whereas it was ten times higher just before, after a day of rain (day 2). Furthermore, as the metallic micropollutants Cd, Cu, Pb and Zn are very well retained by the Rainclean, it can be seen that these elements, once desorbed during dry weather, adsorb onto the Rainclean® located below the sand and deposit (Figure 19, Figure 20, Figure 22, Figure 23). The Rainclean® layer must therefore be positioned below the sand layer, allowing the deposit to develop on the sand layer and not the Rainclean® layer, so that it maintains its adsorbent properties and compensates for any potential desorption that may occur upstream.

It is therefore not advisable to supply water with concentrations that differ greatly from one batch to the next, especially when high concentrations of micropollutants have been applied for at least one day, leading to strong adsorption, followed by low concentrations, resulting in release at the outlet of the treatment plant.

Filter 2 (Rainclean®)	
A) Cd concentration	B) Cd adsorbed

End of day D1 of dry weather

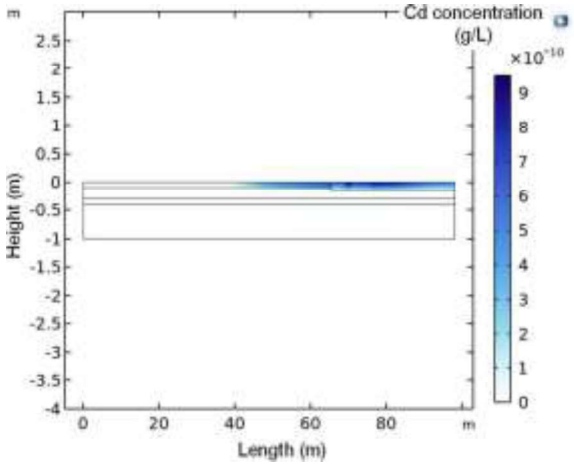

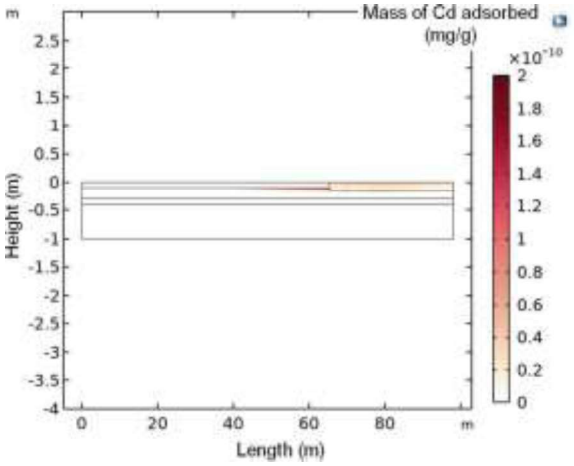

End of day D2 of rain weather

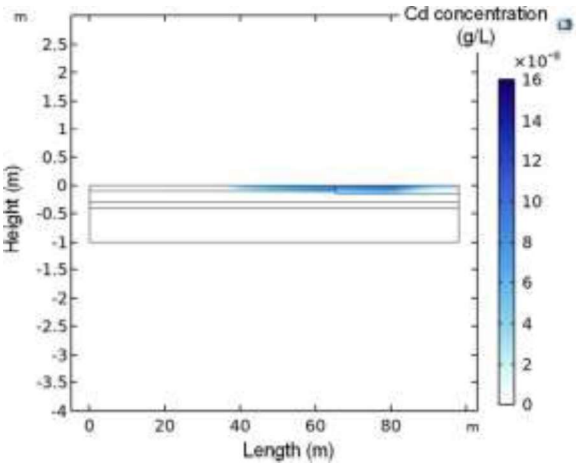

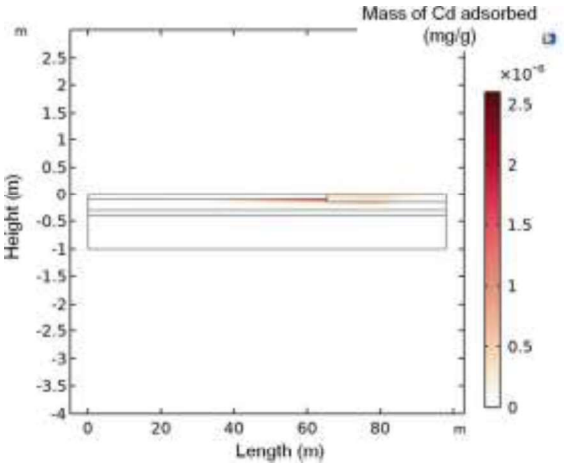

End of day D3 of dry weather

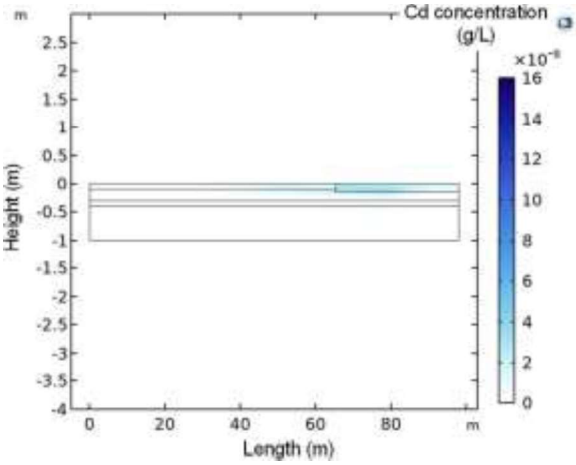

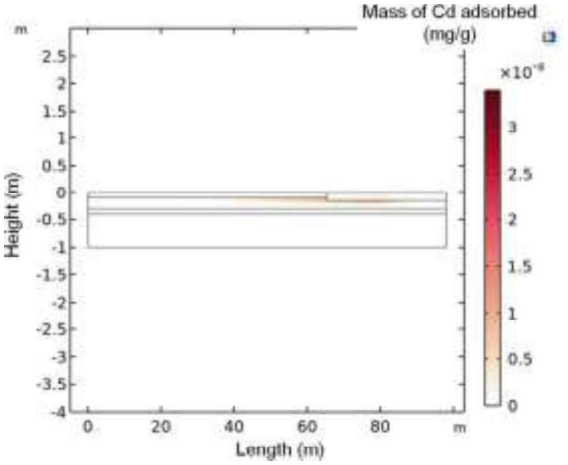

End of day D4 and D5 of rain weather

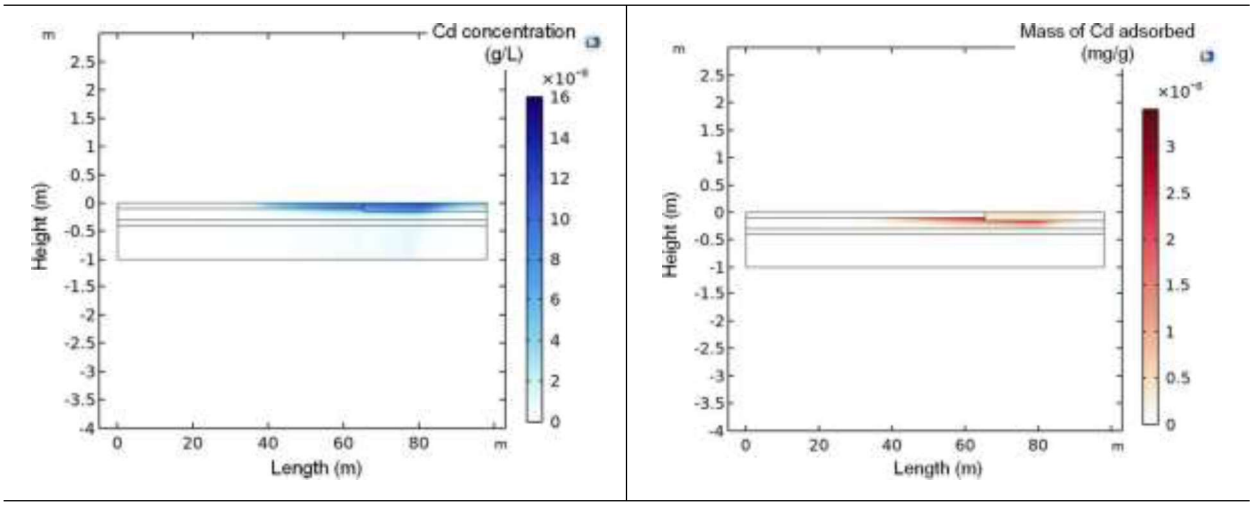

End of day D6 of dry weather

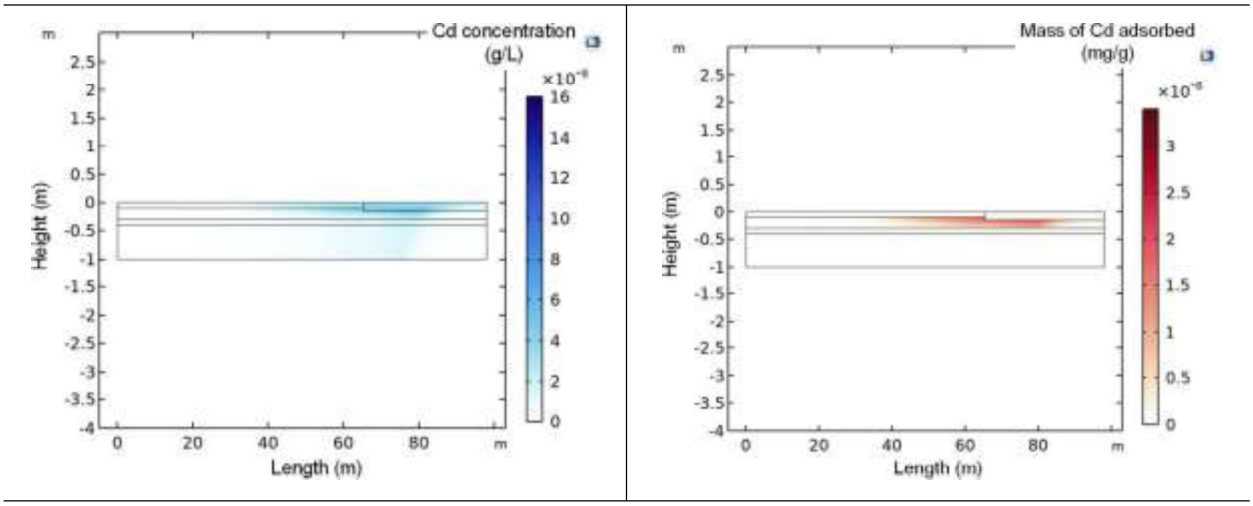

Figure 19: Evolution of the distribution of the concentration (A) and adsorbed mass (B) of Cd in filter 2 at different simulation times when alternating between 'dry weather' and 'rain weather' modes

Filter 2 (Rainclean®)	
A) Cu concentration	B) Cu adsorbed

End of day D1 of dry weather

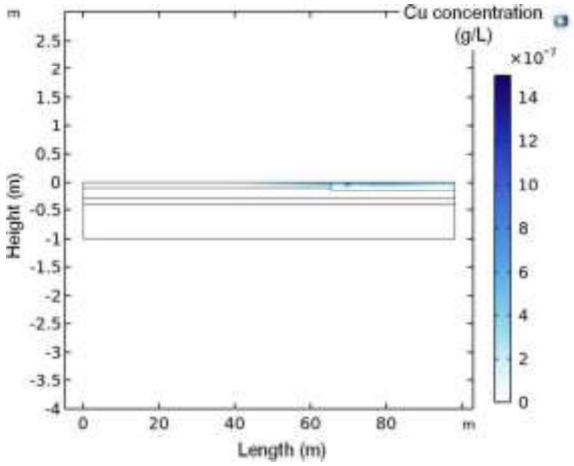

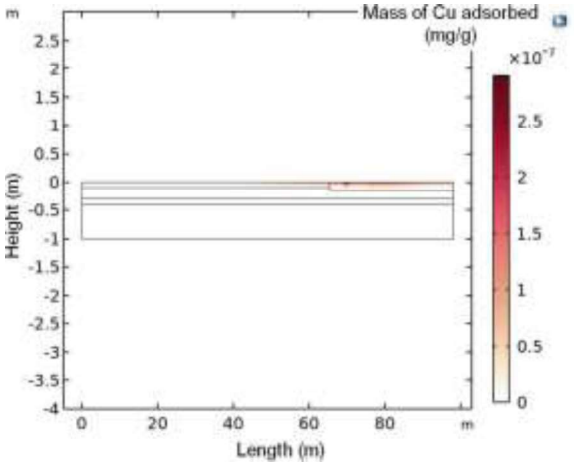

End of day D2 of rain weather

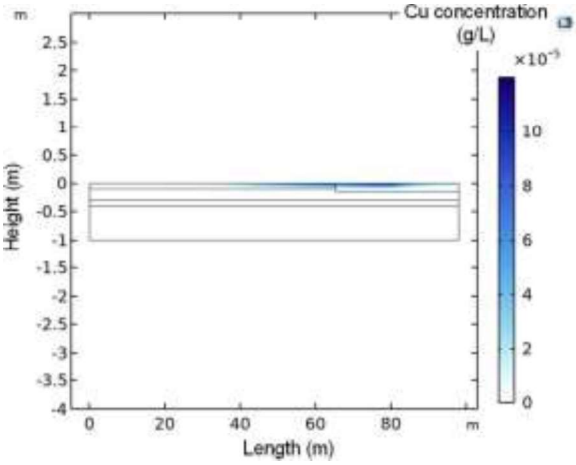

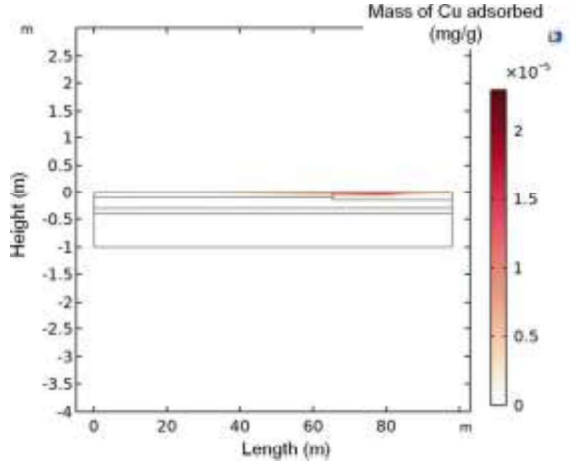

End of day D3 of dry weather

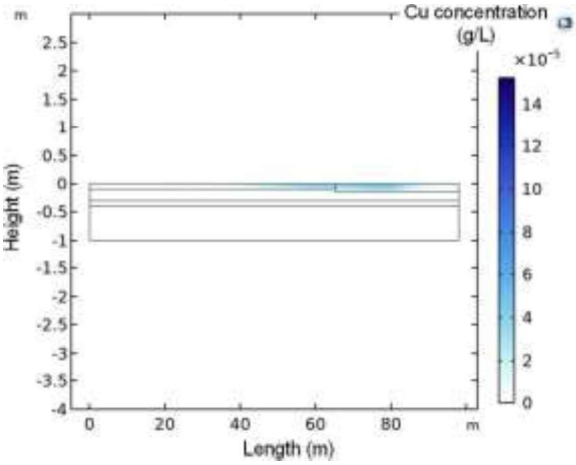

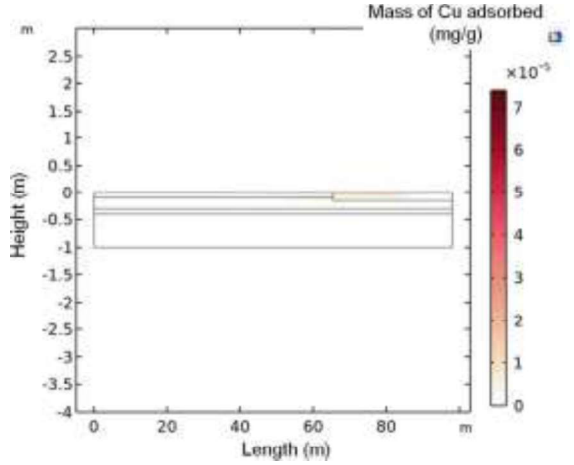

End of day D4 and D5 of rain weather

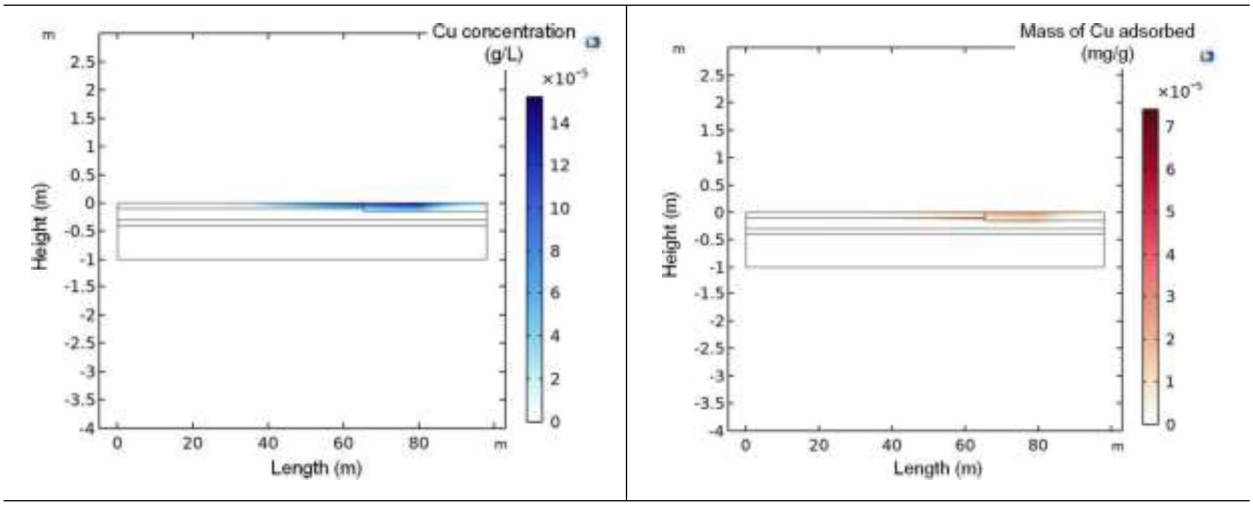

End of day D6 of dry weather

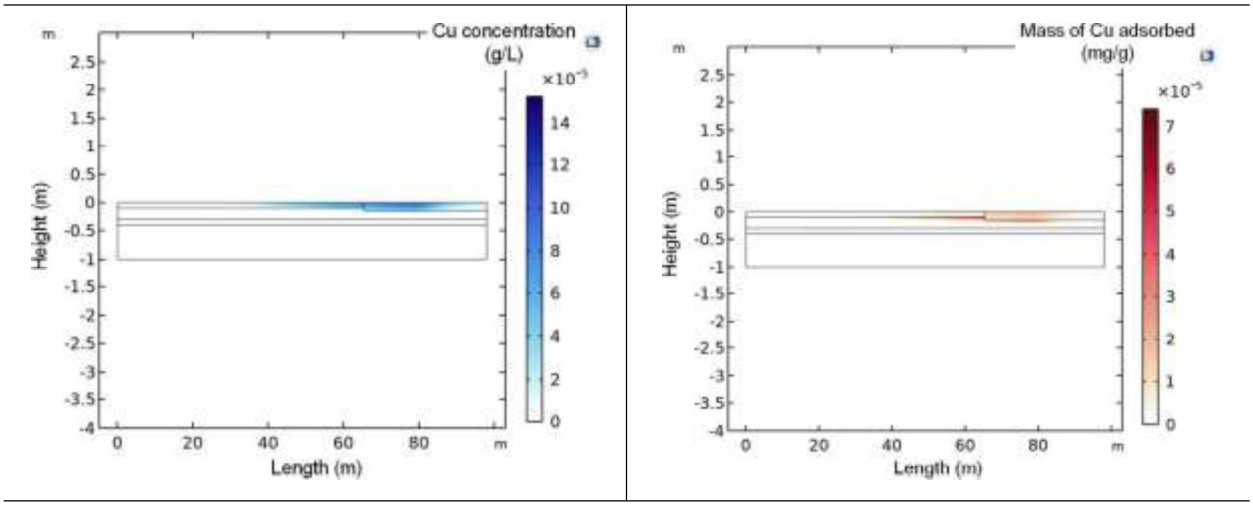

Figure 20: Evolution of the distribution of the concentration (A) and adsorbed mass (B) of Cu in filter 2 at different simulation times when alternating between 'dry weather' and 'rain weather' modes

Filter 2 (Rainclean®)	
A) Ni concentration	B) Ni adsorbed

End of day D1 of dry weather

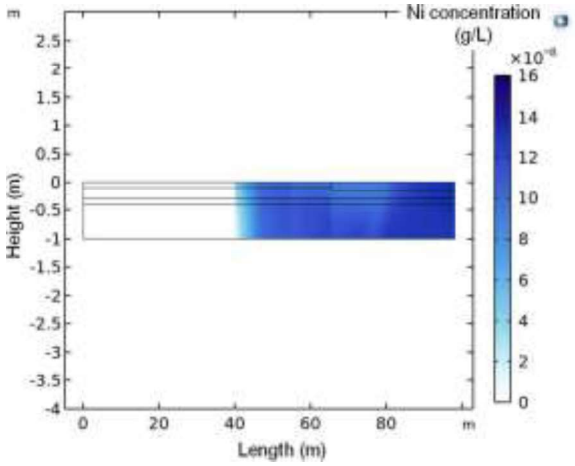

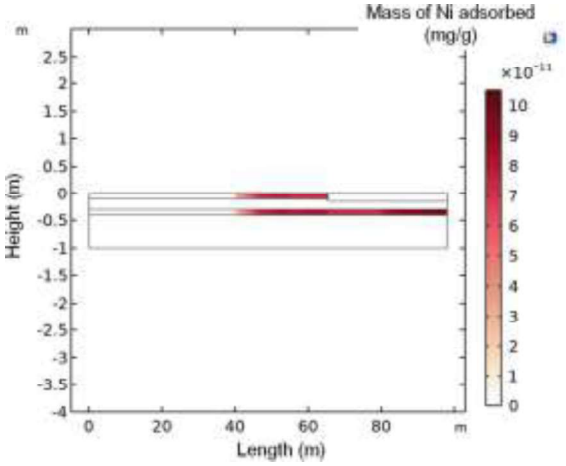

End of day D2 of rain weather

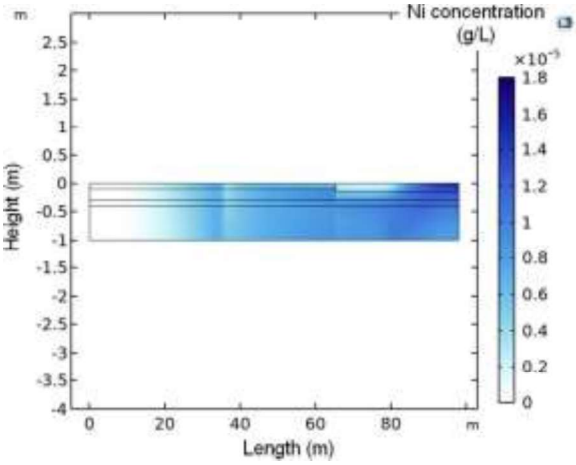

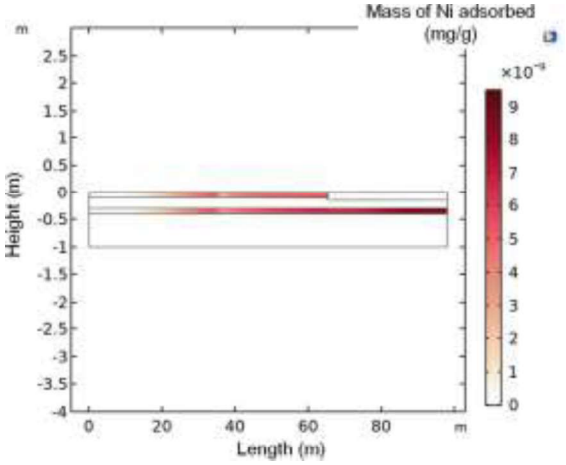

End of day D3 of dry weather

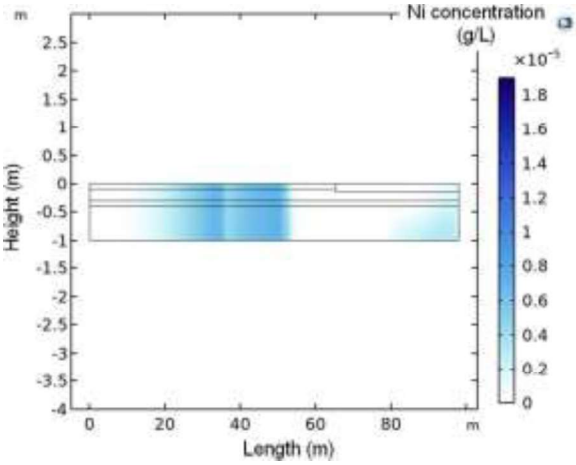

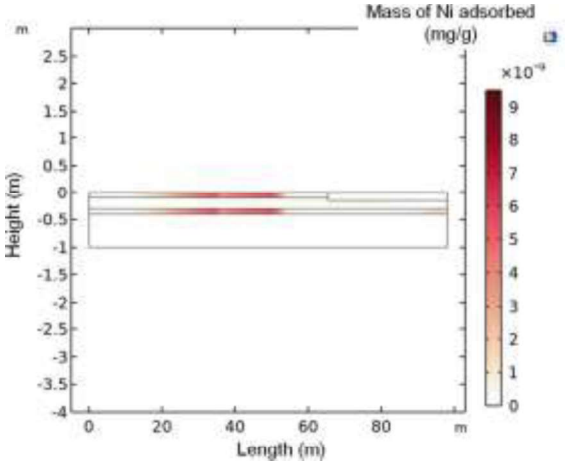

End of day D4 and D5 of rain weather

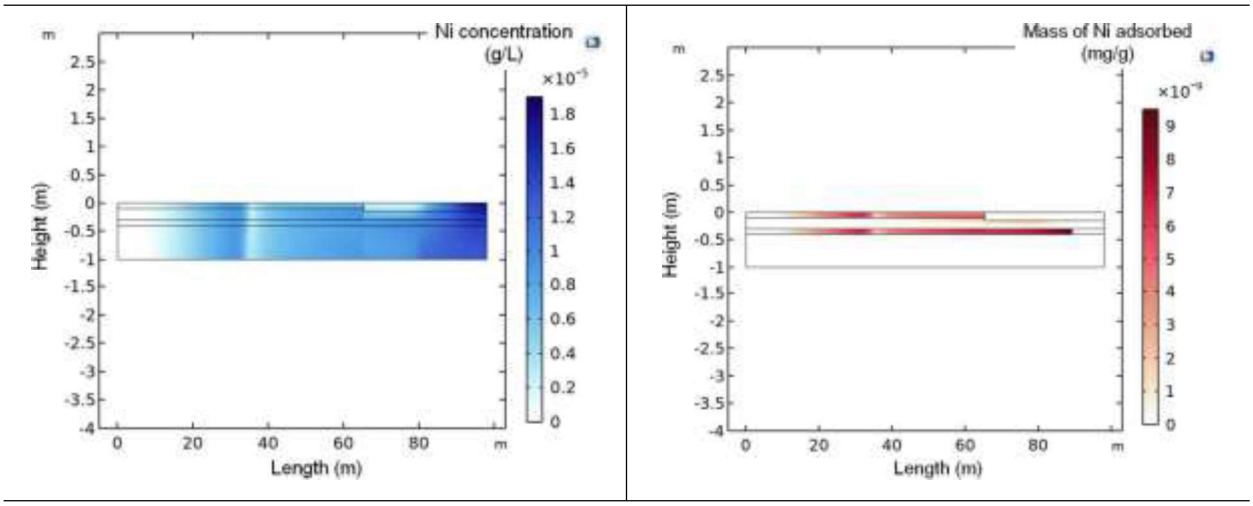

End of day D6 of dry weather

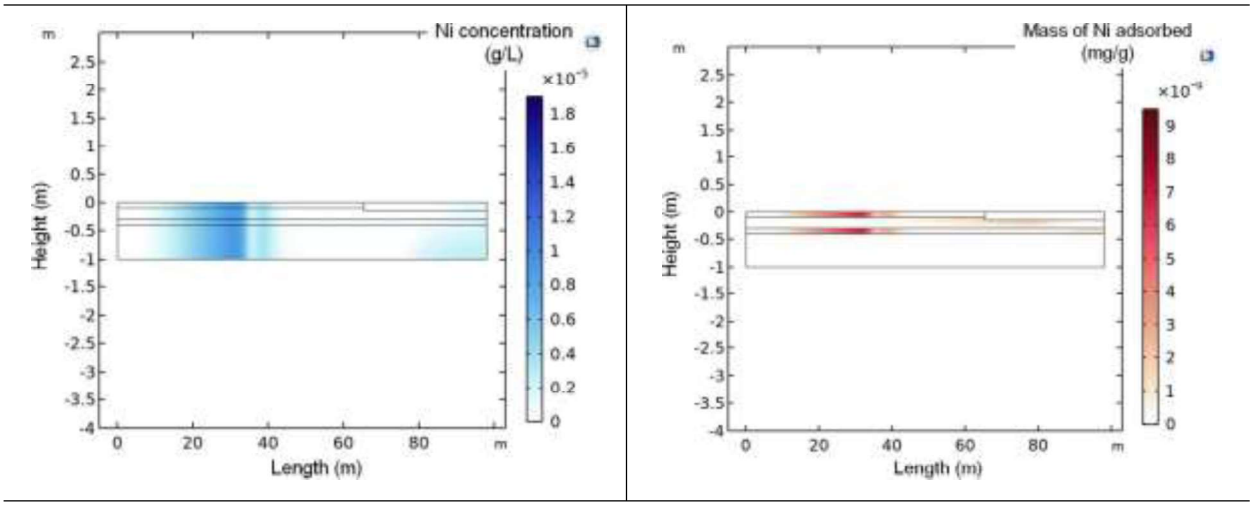

Figure 21: Evolution of the distribution of the concentration (A) and adsorbed mass (B) of Ni in filter 2 at different simulation times when alternating between 'dry weather' and 'rain weather' modes

Filter 2 (Rainclean®)	
A) Pb concentration	B) Pb adsorbed

End of day D1 of dry weather

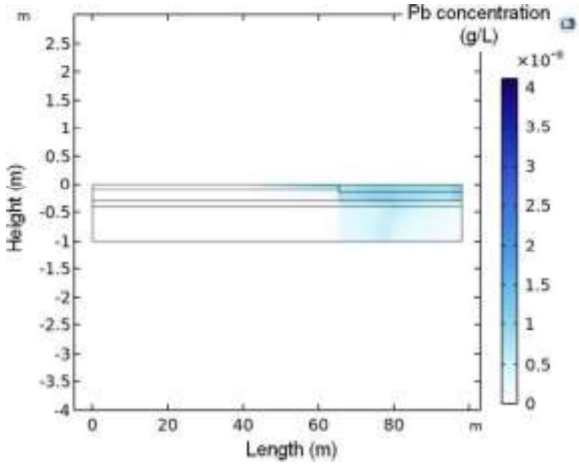

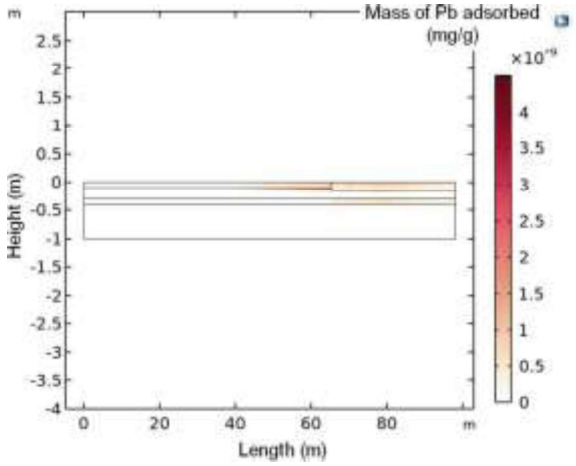

End of day D2 of rain weather

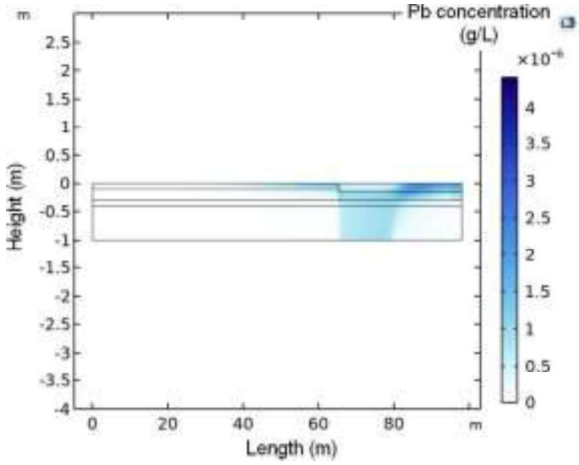

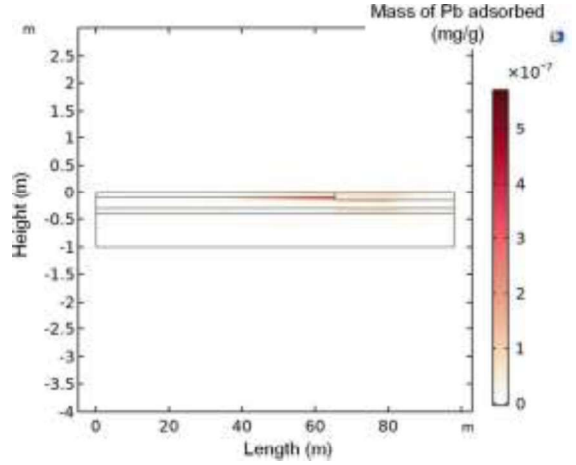

End of day D3 of dry weather

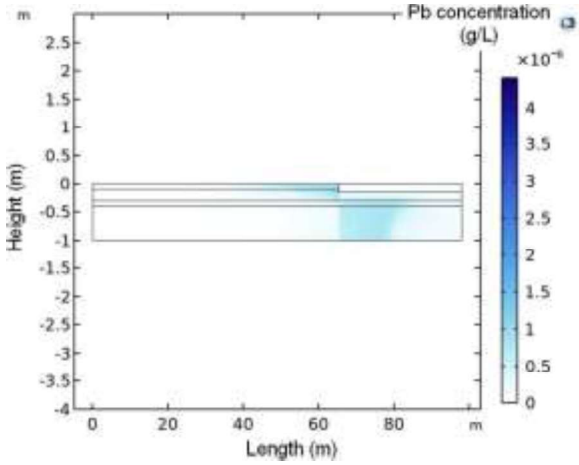

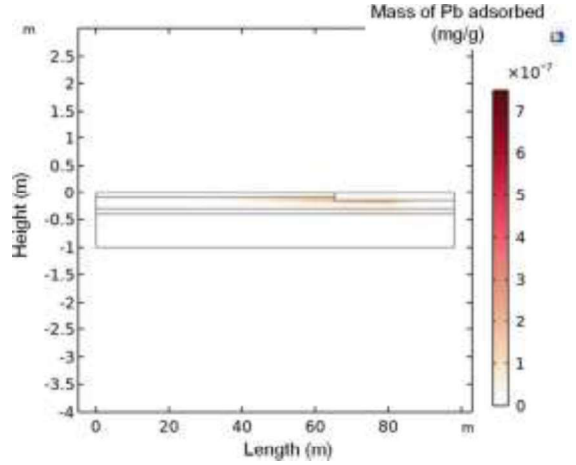

End of day D4 and D5 of rain weather

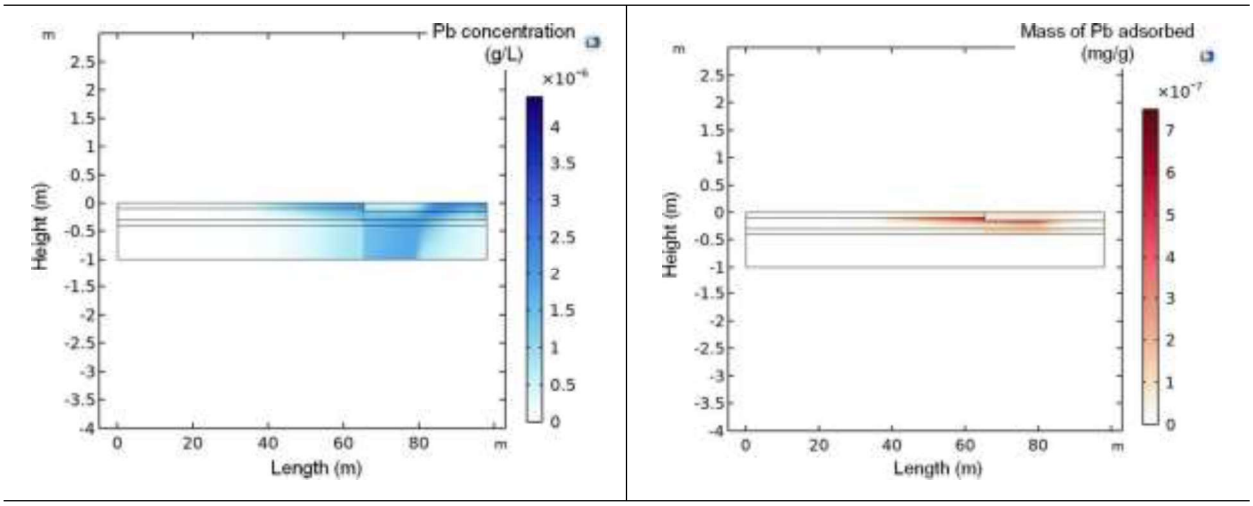

End of day D6 of dry weather

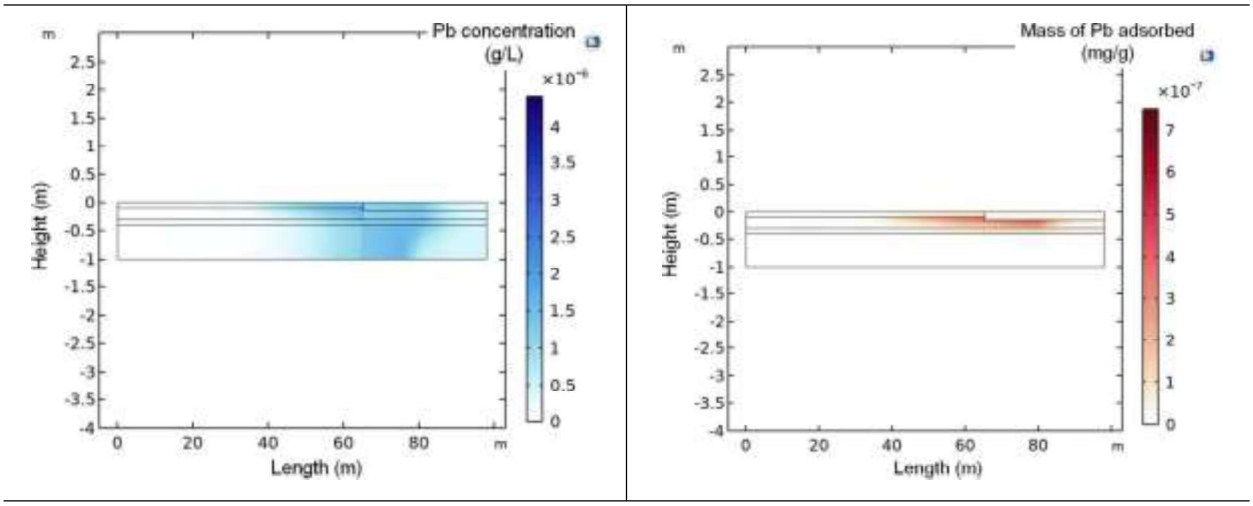

Figure 22: Evolution of the distribution of the concentration (A) and adsorbed mass (B) of Pb in filter 2 at different simulation times when alternating between 'dry weather' and 'rain weather' modes

Filter 2 (Rainclean®)	
A) Zn concentration	B) Zn adsorbed

End of day D1 of dry weather

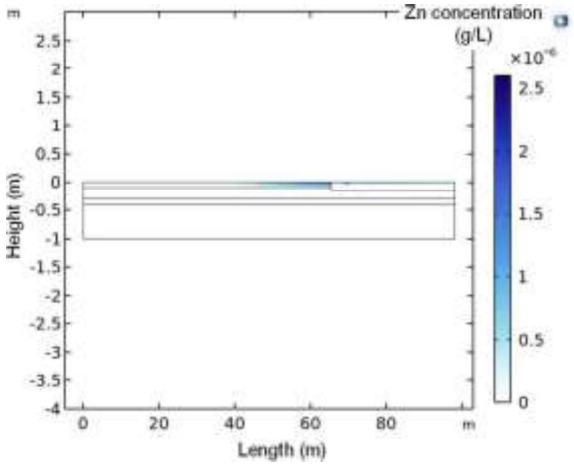

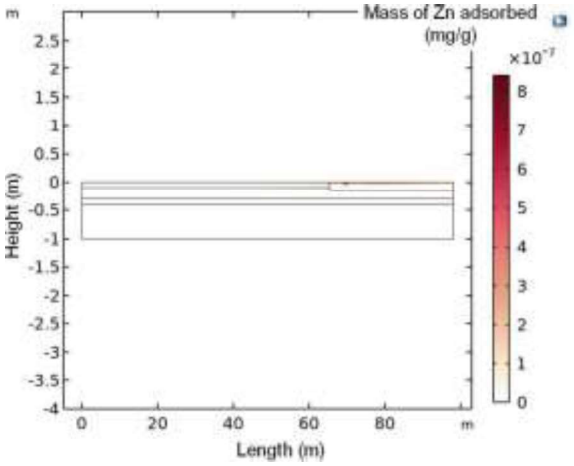

End of day D2 of rain weather

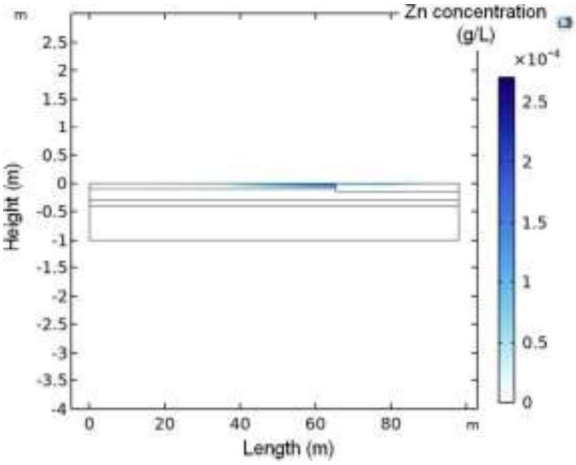

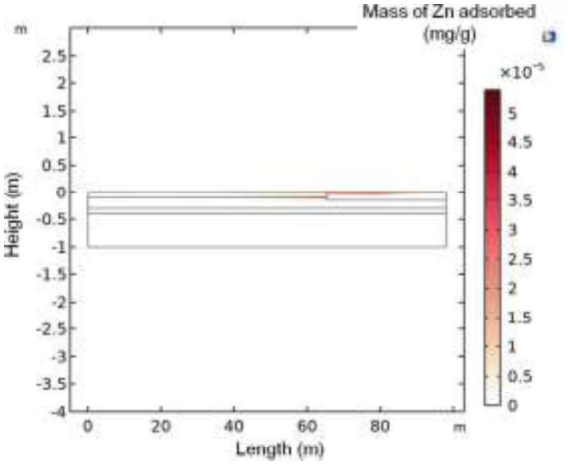

End of day D3 of dry weather

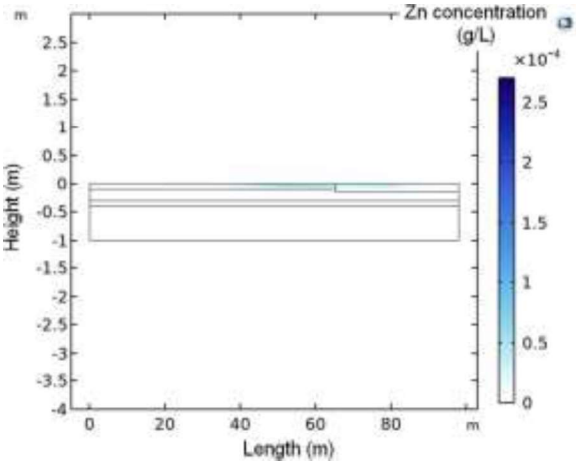

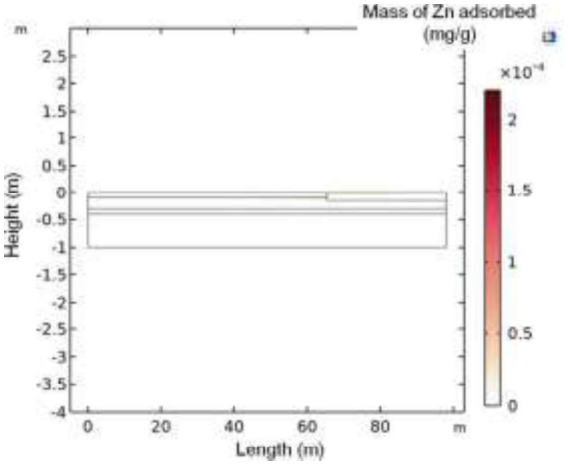

End of day D4 and D5 of rain weather

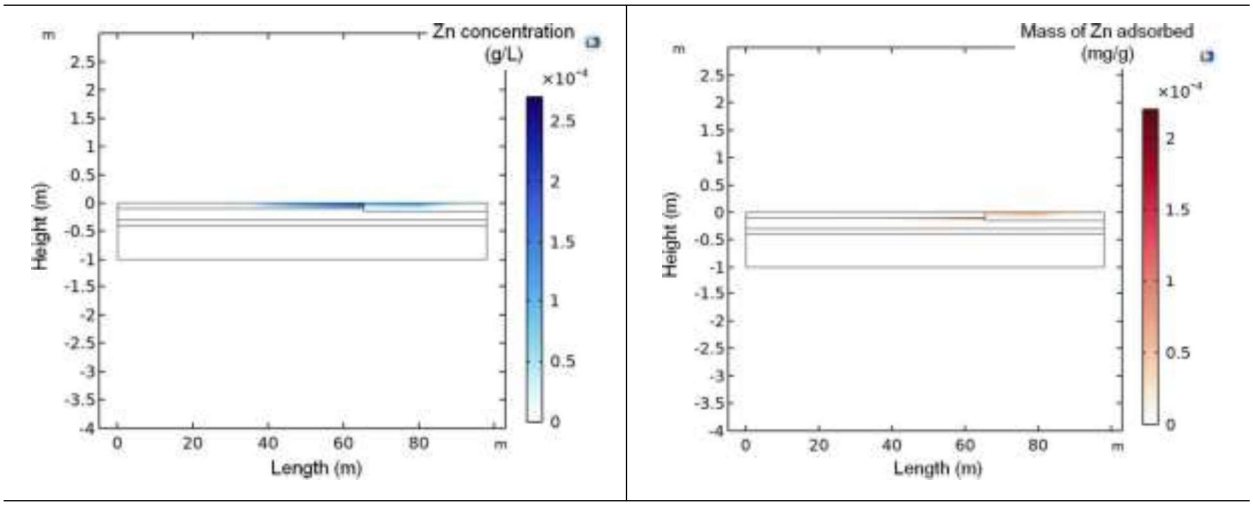

End of day D6 of dry weather

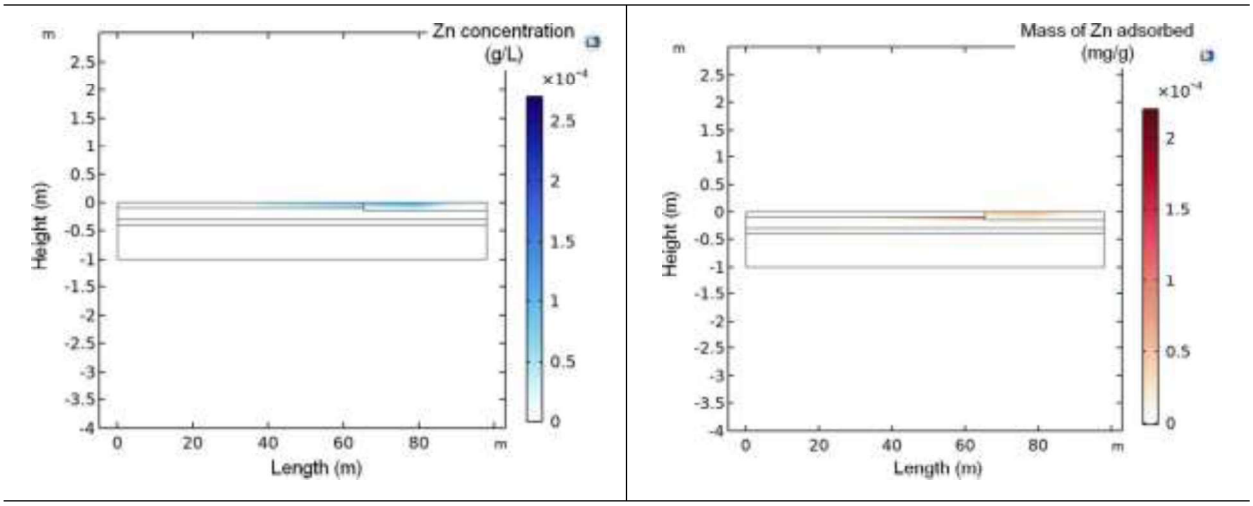

Figure 23: Evolution of the distribution of the concentration (A) and adsorbed mass (B) of Zn in filter 2 at different simulation times when alternating between 'dry weather' and 'rain weather' modes

Filter 2 (Rainclean®)	
A) BPA concentration	B) BPA adsorbed

End of day D1 of dry weather

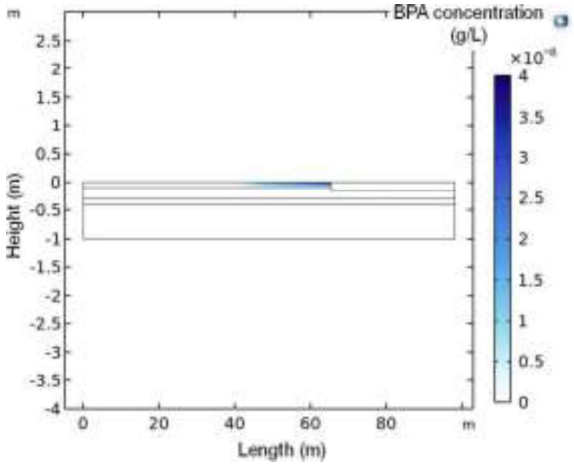

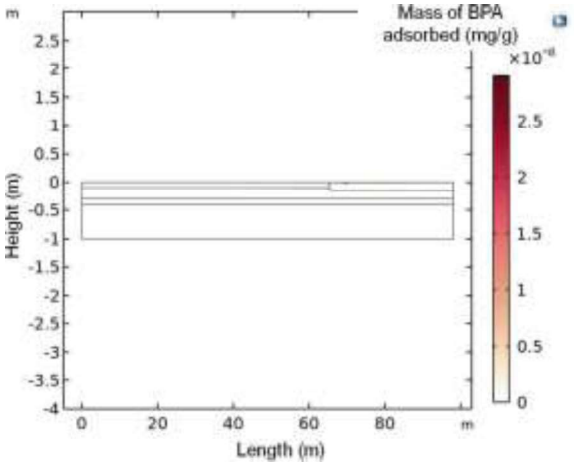

End of day D2 of rain weather

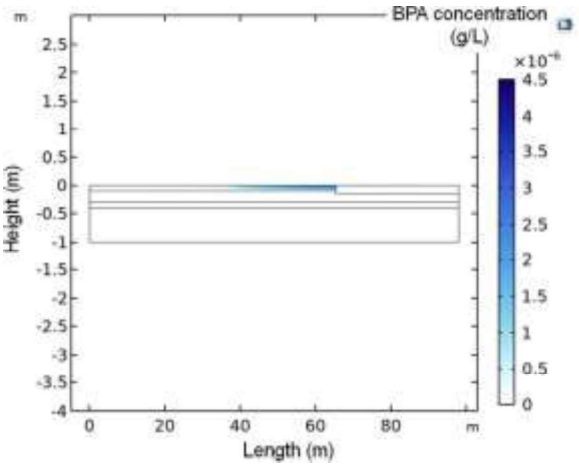

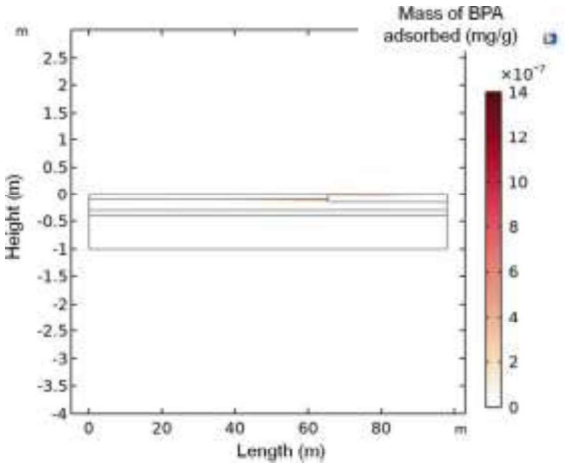

End of day D3 of dry weather

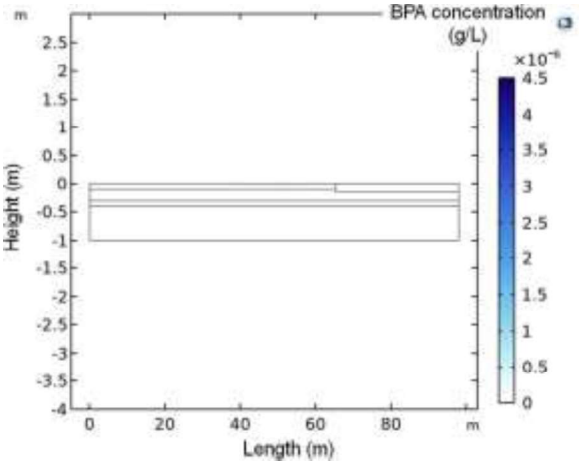

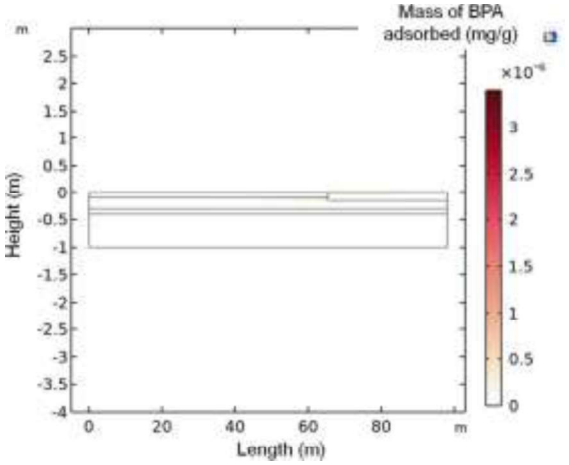

End of day D4 and D5 of rain weather

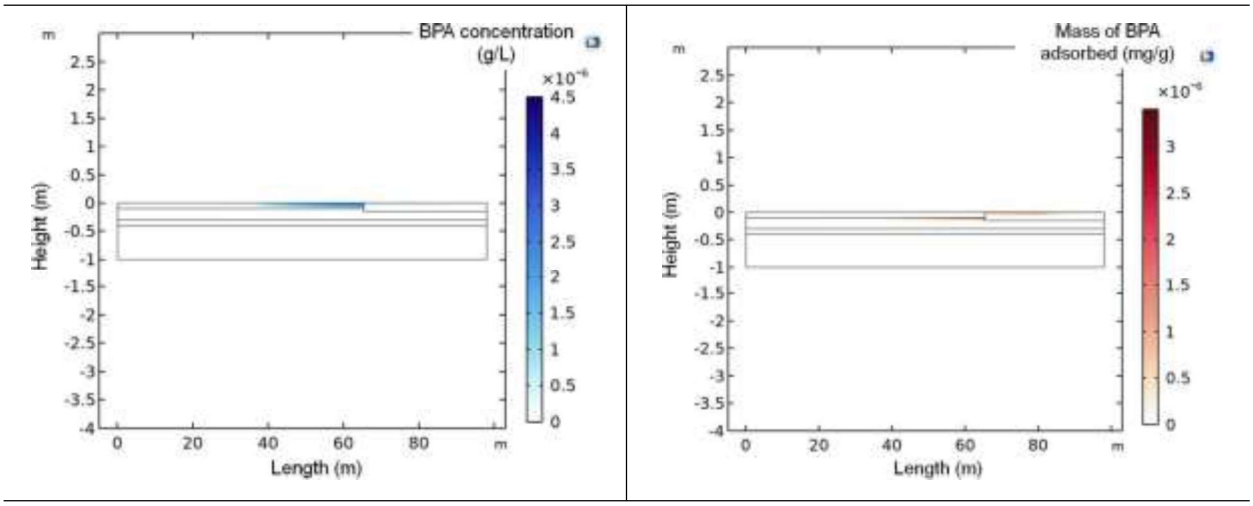

End of day D6 of dry weather

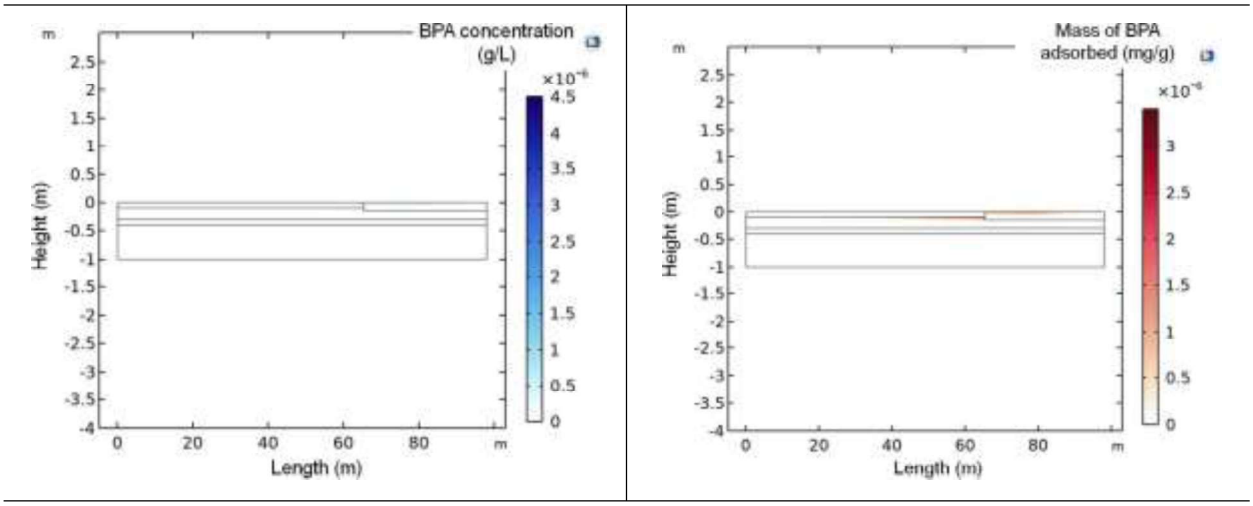

Figure 24: Evolution of the distribution of the concentration (A) and adsorbed mass (B) of BPA in filter 2 at different simulation times when alternating between 'dry weather' and 'rain weather' modes

Filter 2 (Rainclean®)	
A) OP concentration	B) OP adsorbed

End of day D1 of dry weather

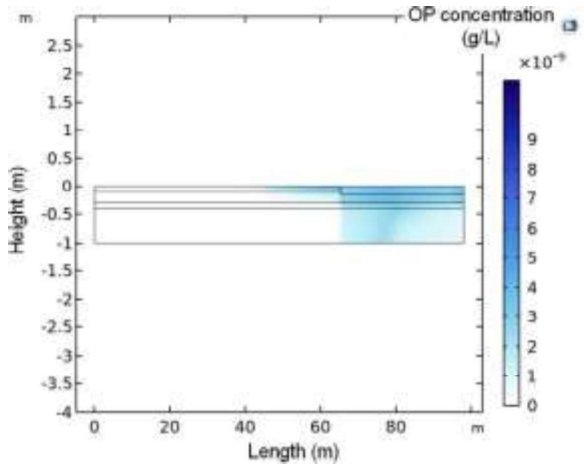

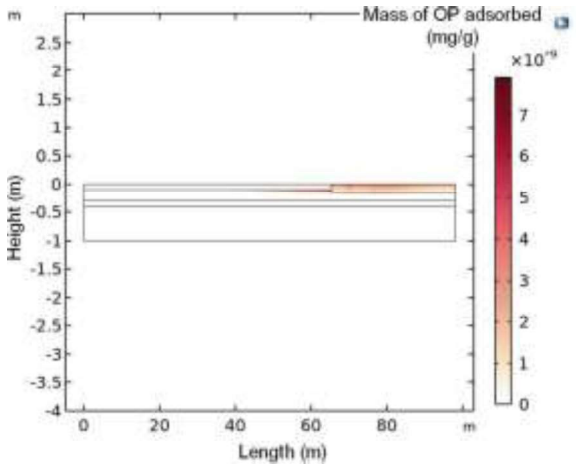

End of day D2 of rain weather

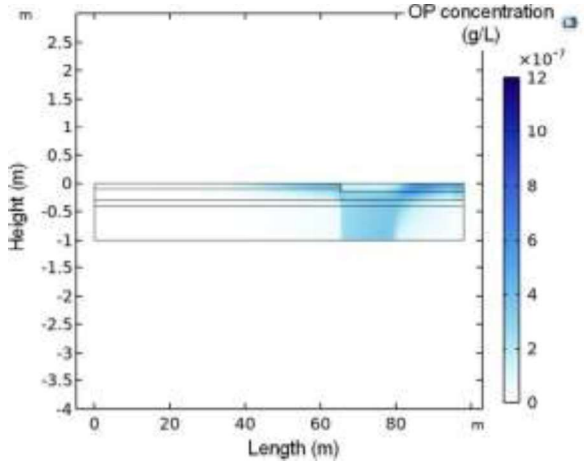

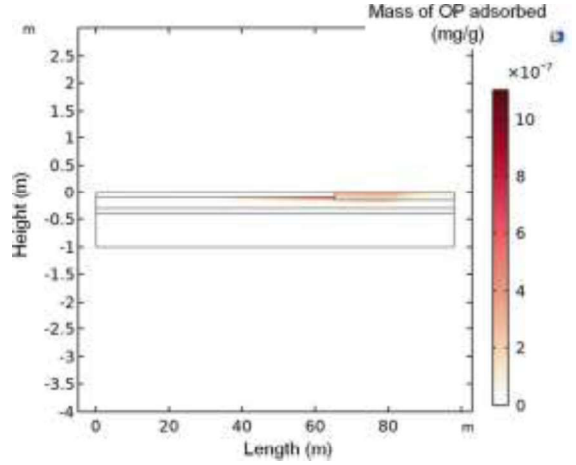

End of day D3 of dry weather

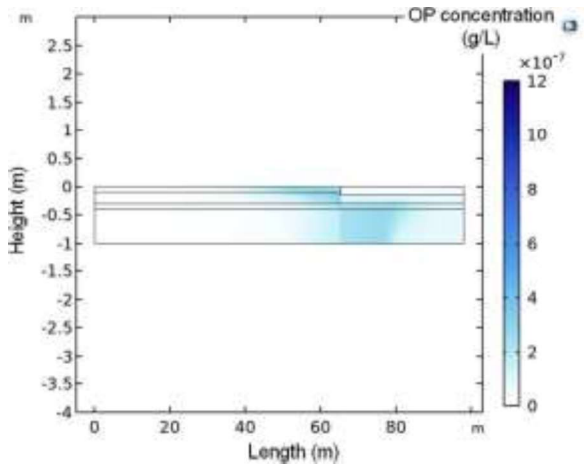

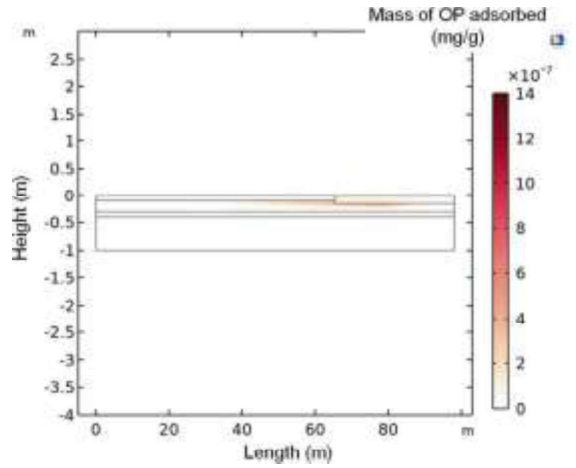

End of day D4 and D5 of rain weather

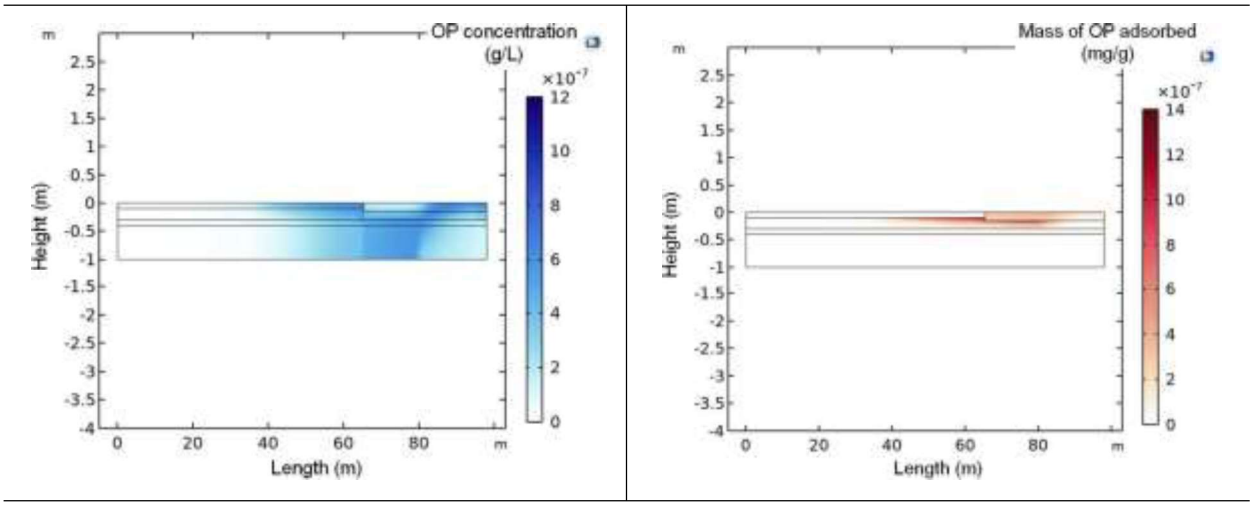

End of day D6 of dry weather

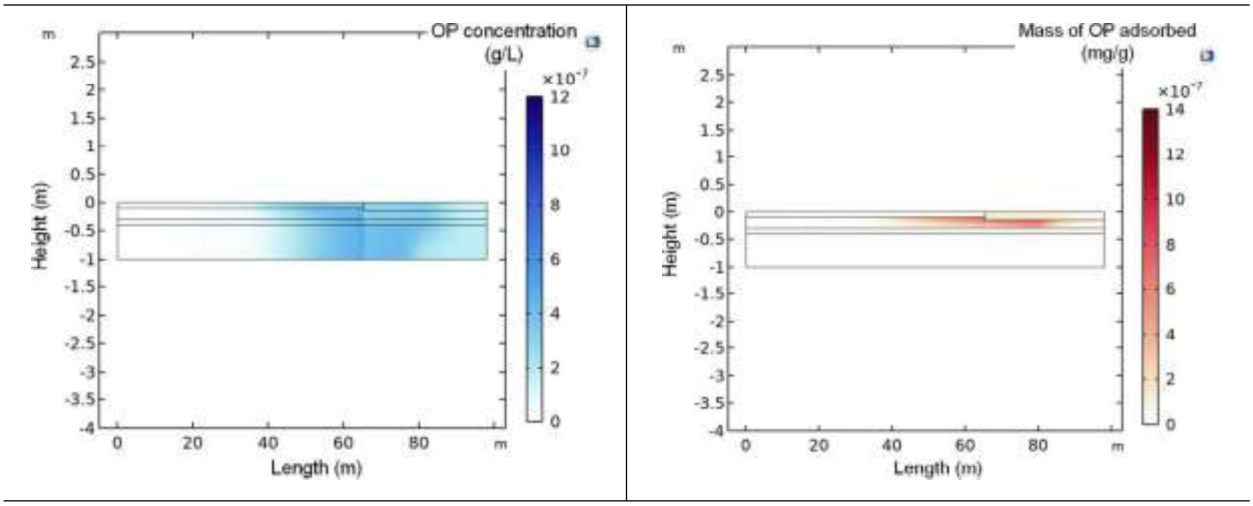

Figure 25: Evolution of the distribution of the concentration (A) and adsorbed mass (B) of OP in filter 2 at different simulation times when alternating between 'dry weather' and 'rain weather' modes

Filter 2 (Rainclean®)	
A) NP concentration	B) NP adsorbed

End of day D1 of dry weather

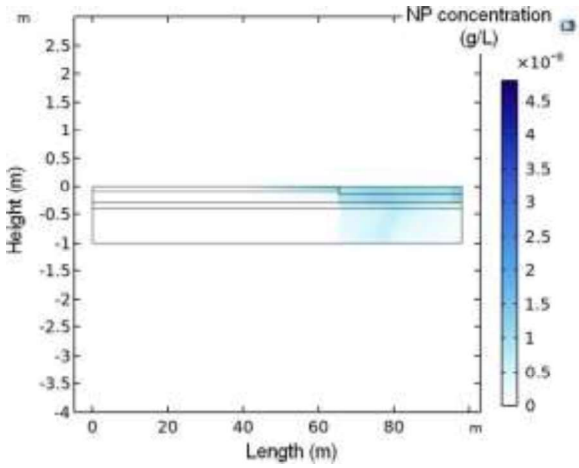

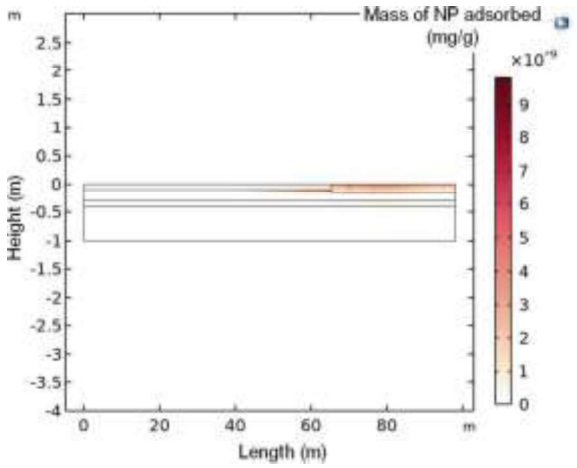

End of day D2 of rain weather

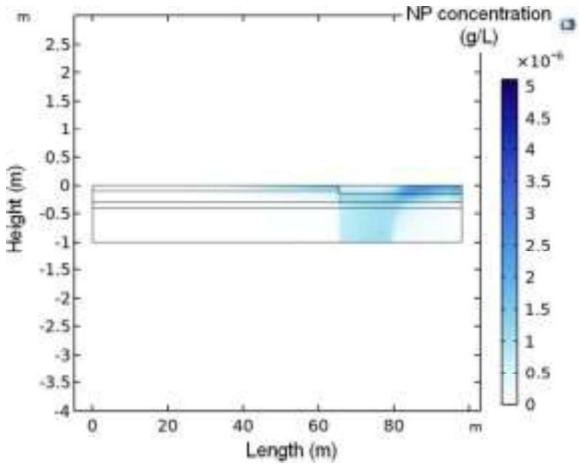

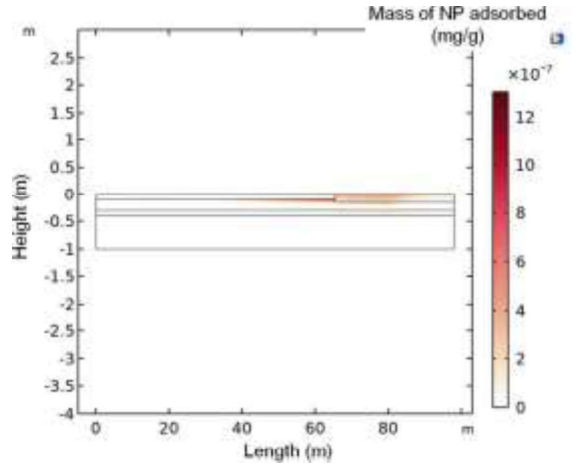

End of day D3 of dry weather

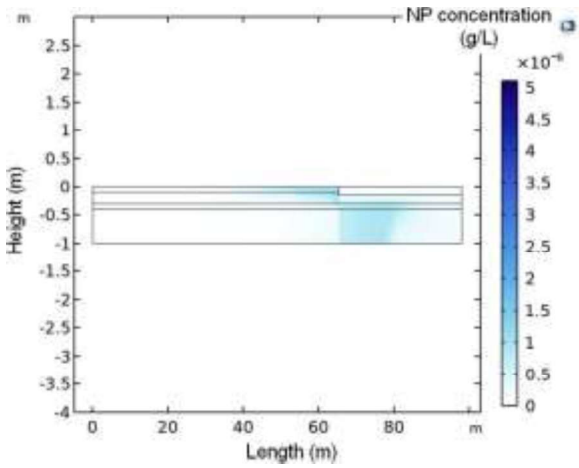

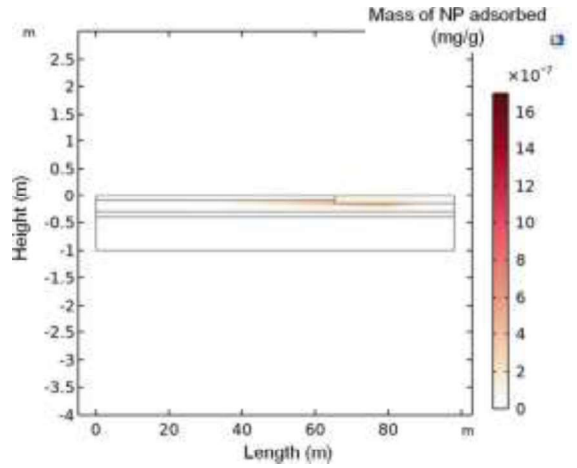

End of day D4 and D5 of rain weather

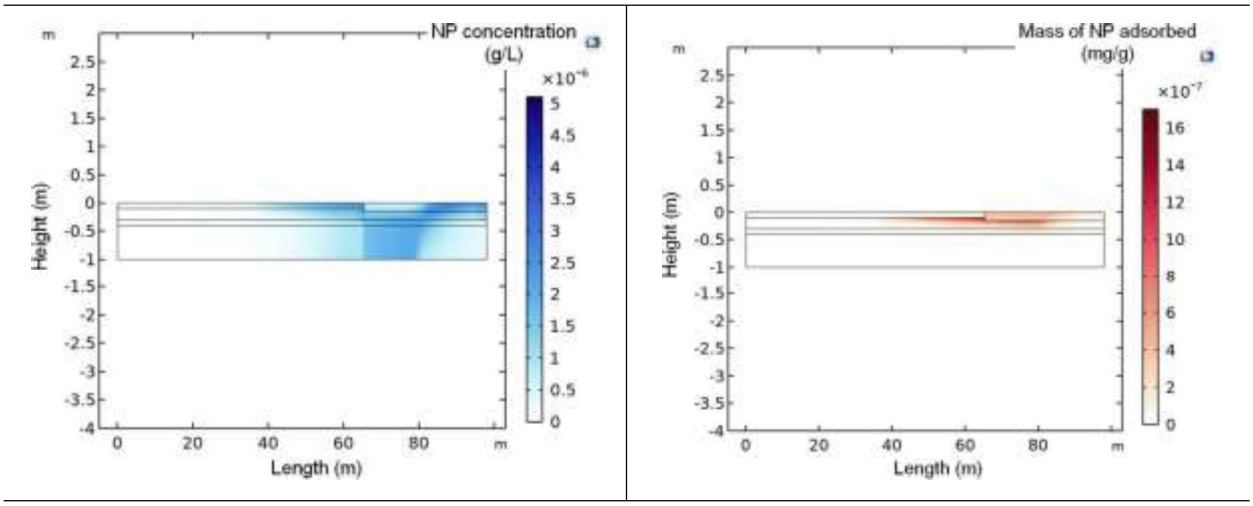

End of day D6 of dry weather

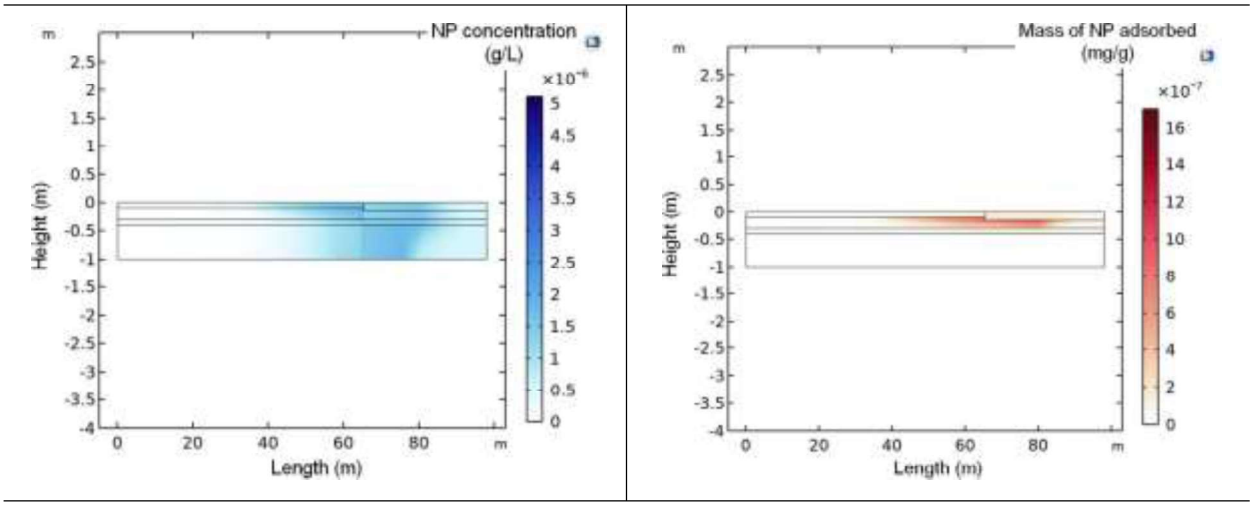

Figure 26: Evolution of the distribution of the concentration (A) and adsorbed mass (B) of NP in filter 2 at different simulation times when alternating between 'dry weather' and 'rain weather' modes

6 Conclusion

Two constructed wetlands were studied to assess their performance in treating stormwater runoff, particularly micropollutants, under both dry and rain weather conditions using simulation models. The filters were nearly identical, except for the filtration layer: Filter 1 included 40 cm of sand, while Filter 2 used 20 cm of the micropollutant-adsorbing material Rainclean®, sandwiched between two 10 cm layers of sand.

Both filters were long (100 m) and uniquely fed at one single point at one end, with an undersized drainage network. These particularities required the use of multiple sub-models to accurately represent flow dynamics.

Tracer experiments (conducted under dry and rain conditions) were simulated for both filters, showing three distinct zones: a dead zone (without drainage), an active zone, and a bypassed zone, highlighting uneven flow and surface use. In Filter 2, overloaded zones were observed where micropollutant accumulation could reduce long-term treatment efficiency.

A simulation with uniform inflow over the entire surface showed that this approach would promote better distribution of flow, reduce dead zones, and improve filter performance, especially when combined with a properly dimensioned drainage network.

When simulating alternating dry and rainy days with variable micropollutant loads, Filter 2 exhibited adsorption during high-load rainy periods, and desorption during dry periods when inflowing water was cleaner. This behavior suggests that large fluctuations in micropollutant concentrations between batches should be avoided, as they can lead to unwanted releases at the outlet.

Finally, desorbed micropollutants during dry weather were shown to re-adsorb onto the Rainclean® layer located below the sand and the deposit. This justifies the strategic placement of the Rainclean® beneath the sand, allowing deposits to accumulate on the sand and preserving the adsorptive capacity of the Rainclean® layer for future micropollutant capture.

7 References

Appelo, Cees Antonius Jacobus, and Dieke Postma. (1993) Geochemistry, Groundwater and Pollution. Balkema, Rotterdam. https://doi.org/10.1017/S0016756800011523.

Bear, Jacob. (1972). Dynamics of fluids in porous media. American Elsevier publishing company, inc., 764 pp.

Bittelli, Marco, Gaylon S. Campbell, and Fausto Tomei. *Soil Physics with Python: Transport in the Soil–Plant–Atmosphere System*. Oxford University Press, 2015. https://doi.org/10.1093/acprof:oso/9780199683093.001.0001.

Domenico, Paul A., and Franklin W. Schwartz. (1990). Physical and Chemical Hydrogeology. John Wiley and Sons, New York, 807 pp.

Gromaire, Marie-Christine, Julie Gasperi, Sophie Deshayes, Sophie Ayrault, Pierre Labadie, Kate Flanagan, Laurent Varnede, Maïssae Saad, Emilie Caupos, Christine Partibane, Leila Boudahmane, Laurent Meffray, Dominique Demare, Julie Paupardin, and Philippe Neveu. (2022). Micropollutant screening of road and parking runoff in Paris conurbation. Mendeley Data, V1. https://doi.org/10.17632/m8kcmthfd2.1.

Meles, Menberu B., Lin Chen, Carl Unkrich, Hoori Ajami, Scott A. Bradford, Jiří Šimůnek, and Dave C. Goodrich. "Computationally Efficient Watershed-Scale Hydrological Modeling: Integrating HYDRUS-1D and KINEROS2 for Coupled Surface-Subsurface Analysis." *Journal of Hydrology* 640 (August 1, 2024): 131621. https://doi.org/10.1016/j.jhydrol.2024.131621.

Li, Tian, Yonghua Fan, Dong Cun, Xiaoyan Song, Yuxin Dai, Fangyuan Wang, Chengjun Wu, and Wenwen Liang. (2020). Treatment performance and microbial response to dibutyl phthalate contaminated wastewater in vertical flow constructed wetland mesocosms. Chemosphere, 246, 125635. https://doi.org/10.1016/j.chemosphere.2019.125635.

Morvannou, Ania, Matthieu Dufresne, Marie-Christine Gromaire, Stéphane Troesch, and Nicolas Forquet. "Sizing Efficient Underdrains for Treatment Wetlands." *Water Science and Technology* 89, no. 2 (December 22, 2023): 241–51. https://doi.org/10.2166/wst.2023.417.

Qi, Xinying, Tian Li, Fangyuan Wang, Yuxin Dai, and Wenwen Liang. (2018). Removal efficiency and enzymatic mechanism of dibutyl phthalate (DBP) by constructed wetlands. Environmental Science and Pollution Research, 25(23), 23009–23017. https://doi.org/10.1007/s11356-018-2384-5.

Rajabzadeh, Amin Reza, Raymond L. Legge, and Kela P. Weber. "Multiphysics Modelling of Flow Dynamics, Biofilm Development and Wastewater Treatment in a Subsurface Vertical Flow Constructed Wetland Mesocosm." *Ecological Engineering* 74 (January 1, 2015): 107–16. https://doi.org/10.1016/j.ecoleng.2014.09.122.

Samsó, Roger, Joan García, Pascal Molle, and Nicolas Forquet. "Modelling Bioclogging in Variably Saturated Porous Media and the Interactions between Surface/Subsurface Flows: Application to Constructed Wetlands." *Journal of Environmental Management* 165 (January 1, 2016): 271–79. https://doi.org/10.1016/j.jenvman.2015.09.045.

Samsó, Roger, Jordi Blázquez, Núria Agulló, Joan Grau, Ricardo Torres, and Joan García. "Effect of Bacteria Density and Accumulated Inert Solids on the Effluent Pollutant Concentrations Predicted by the Constructed Wetlands Model BIO_PORE." *Ecological Engineering*, Special Issue: 5th international Symposium on Wetland Pollutant Dynamics and Control, 80 (July 1, 2015): 172–80. https://doi.org/10.1016/j.ecoleng.2014.09.069.

Toro-Vélez, Andrés Felipe, Carlos Andrés Madera-Parra, María del Rosario Peña-Varón, Helver García-Hernández, Wai Yin Lee, Scott William Walker, and Piet N.L. Lens. (2017). Longitudinal removal of Bisphenol-A and nonylphenols from pretreated domestic wastewater by tropical horizontal subsurface constructed wetlands. Applied Sciences, 7(8), 834. https://doi.org/10.3390/app7080834.

Torricelli, E. (1644). Opera geometrica, Amatoris Masse & Laurentij de Landis, Florence, Italy

van Genuchten, Martinus Theodorus. (1980). A closed-form equation for predicting the hydraulic conductivity of unsaturated soils. Soil Science Society of America Journal, 44, 892–898. https://doi.org/10.2136/sssaj1980.03615995004400050002x.

Weill, S., E. Mouche, and J. Patin. "A Generalized Richards Equation for Surface/Subsurface Flow Modelling." *Journal of Hydrology* 366, no. 1 (March 15, 2009): 9–20. https://doi.org/10.1016/j.jhydrol.2008.12.007.

Zhu, Hua, Xiangyu Yu, Yuzhen Xu, Bing Yan, Gerardo Bañuelos, Ben Shutes, and Zhiguo Wen. (2021). Removal of chlorpyrifos and its hydrolytic metabolite in microcosm-scale constructed wetlands under soda saline-alkaline condition: mass balance and intensification strategies. Science of the Total Environment, 777, 145956. https://doi.org/10.1016/j.scitotenv.2021.145956.

Zhu, Wei-Lei, Li-Hua Cui, Yi Ouyang, Chang-Fu Long, and Xiao-Dong Tang. (2022). Kinetic adsorption of ammonium nitrogen by substrate materials for constructed wetlands. Pedosphere, 21(3), 454–463. https://doi.org/10.1016/S1002-0160(11)60147-1.

8 Appendixe: Bugeaud treatment wetlands

8.1 Description

The two treatment wetlands under consideration (hereafter referred to as "treatment wetlands" or "filters") are located in the Bois de Boulogne in Paris. The primary design objective of these systems is stormwater treatment, with a particular emphasis on the removal of metallic and organic micropollutants. The collection of stormwater is predominantly sourced from the Parisian ring (Boulevard Périphérique). The stormwater is initially accumulated in a designated storage basin. From there, it is transferred to a pumping station, where it is then discharged onto the treatment wetlands. The effluent from the treatment wetlands is discharged into a pond, and subsequently into a stream that ultimately flows into the Seine River (Figure 27).

Figure 27. Water flow, from the Paris ring road to the filters and then to the Seine

Figure 28 presents a top-level view of the two treatment wetlands at the Bugeaud site. Each wetland is planted with *Phragmites australis* and has a unitary surface area of 600 m² (98 m in length, 6.12 m in width, and 1 m in depth). Both filters are operated in a similar manner and are fed in an alternating sequence. The alternance occurs after one month of operation. A single feeding point is located at one end of the treatment wetland. The manhole that collects the effluent is located on the opposite end.

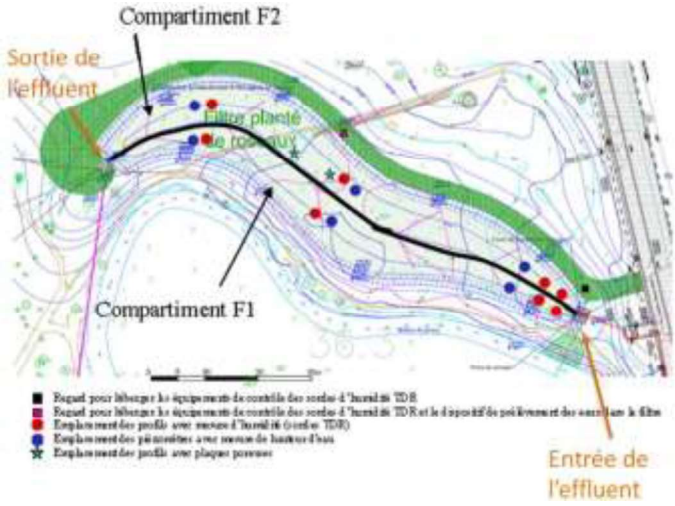

Figure 28. Top-level view of the Bugeaud treatment wetland

The filters are composed of the following layers, from top to bottom: a 40-centimeter-thick filtration layer, a 10-centimeter-thick transition layer where aeration underdrains have been placed, and a 50-centimeter-thick drainage layer. Both filters feature identical drainage and transition layers. However, filter 1 utilizes a sand filtration layer (0/4 mm), while filter 2 employs a more complex design with three distinct sublayers. The top and bottom layers of filter 2 are composed of 10-centimeter-thick sand layers, with a 20-centimeter-thick layer of Rainclean®, an adsorbent material specifically engineered for stormwater treatment, sandwiched between them. The sand utilized in both filters is identical. A standpipe is placed at the outlet of the underdrain network of both filters to maintain the drainage layer's saturation. It features a calibrated opening positioned 30 centimeters from the bottom of the filter. This design is intended to provide a controlled outflow rate (close to 20 L/s). This device enables the maintenance of a water volume in the filter of up to 72 m³ of the total 180 m³ of the drainage layer (assuming a porosity of 40%). This volume provides an accessible storage solution for Phragmites australis, effectively mitigating hydric stress during both the dry and resting periods. The annual volume of water to be treated is estimated at 200,000 cubic meters. This water is comprised of stormwater from the Parisian ring (with a catchment area of 21 hectares), extraneous water (279 cubic meters per day), and a small volume (few percent of the yearly volume) of combined sewer overflow from a network that drains a catchment area of 71 hectares. The influent is collected in a 3,500-cubic-meter storage basin before flowing to a pumping station that supplies the filters.

8.2 Monitoring

A variety of measurement techniques have been employed to evaluate the hydrodynamics of the filters and their effectiveness in removing pollutants. For the flow modeling component, we will rely on flow rate measurements, water height, and water content (Figure 29). To model micropollutant transport, the relevant measurements are the inlet and outlet concentrations of pollutants, as well as the samples collected within the porous media using suction plates (Figure 29).

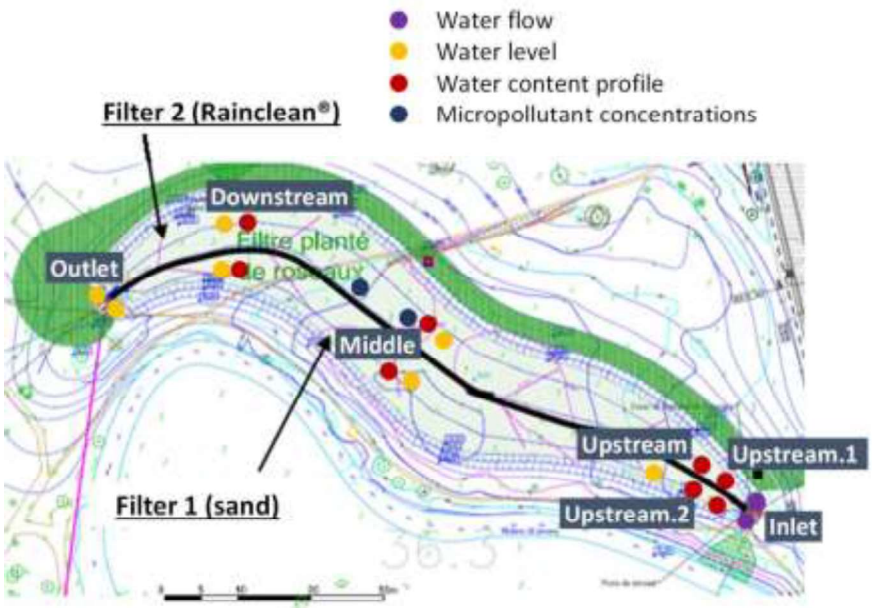

Figure 29. Location of sensors and sampling points